ISOSPIN DEPENDENT ENTRAINMENT IN ROTATING SUPERFLUID NEUTRON STARS

By
APURBA KHETO
PHYS05201104002

Saha Institute of Nuclear Physics, Kolkata

A thesis submitted to the

Board of Studies in Physical Sciences

In partial fulfillment of requirements
For the Degree of
DOCTOR OF PHILOSOPHY
of
HOMI BHABHA NATIONAL INSTITUTE

November, 2015

Homi Bhabha National Institute

Recommendations of the Viva Voce Board

As members of the Viva Voce Board, we certify that we have read the dissertation prepared by **Apurba Kheto** entitled **"Isospin Dependent Entrainment in Rotating Superfluid Neutron Stars"** and recommend that it maybe accepted as fulfilling the dissertation requirement for the Degree of Doctor of Philosophy.

Prof. Parthasarathi Mitra P. Mitra Date: 19.2.16

Chairman

Prof. Debades Bandyopadhyay Debades Bandyopadhyay Date: 19.2.2016

Guide/Convener

Prof. Hiranmaya Mishra Hiranmaya Mishra Date: 19th Feb. 2016

Examiner

Prof. Debasish Majumdar Debasish Majumdar Date: 19/02/2016

Member 1

Prof. Bijay Agrawal Bijay Agrawal Date: 19.2.2016

Member 2

Final approval and acceptance of this dissertation is contingent upon the candidate's submission of the final copies of the dissertation to HBNI.

I hereby certify that I have read this dissertation prepared under my direction and recommend that it may be accepted as fulfilling the dissertation requirement.

Date: 19.2.2016

Place: KOLKATA

Guide: Debades Bandyopadhyay

Prof. Debades Bandyopadhyay

STATEMENT BY AUTHOR

This dissertation has been submitted in partial fulfillment of requirements for an advanced degree at Homi Bhabha National Institute (HBNI) and is deposited in the Library to be made available to borrowers under rules of the HBNI.

Brief quotations from this dissertation are allowable without special permisiion, provided that accurate acknowledgement of source is made. Requests for permission for extended quotation from or reproduction of this manuscript in whole or in part may be granted by the Competent Authority of HBNI when in his or her judgment the proposed use of the material is in the interests of scholarship. In all other instances, however, permission must be obtained from the author.

Apurba Kheto

DECLARATION

I, hereby declare that the investigtion presented in the thesis has been carried out by me. The work is original and has not been submitted eralier as a whole or in part for a degree / diploma at this or any other Institution / University.

Apurba Kheto

List of Publications Arising from the Thesis

Journal

1. Slowly rotating superfluid neutron stars with isospin dependent entrainment in a two-fluid model.

   Apurba Kheto and Debades Bandyopadhyay;

   Physical Review D 91, 043006 (2015) [arXiv:1502.03920]

2. Isospin dependence of entrainment in superfluid neutron stars in a relativistic model.

   Apurba Kheto and Debades Bandyopadhyay;

   Physical Review D 89, 023007 (2014) [arXiv:1308.5567]

Chapters in Books and Lecture Notes: None

Conferences: None

Others: None

Apurba Kheto

To My Parents.......

ACKNOWLEDGEMENTS

First and foremost, I thank my thesis supervisor Prof. Debades Bandyopadhyay for introducing me to the interesting topic of superfluid Neutron star. He has always motivated me and encouraged me to pursue my own line of thinking. This research work was possible only due to the sincere help and support from him. I would like to thank all the other professors of APC and Theory division for their guidance during the entire period of my research.

I would also like to thank my friends and seniors of APC and Theory division, as well as other students in the institute with whom I have shared invaluable moments. I am sincerely thankful to Prasanta and Goutam for their constant support and encouragements and helping me to acquire numerical programming skills.

Finally, I wish to express my deep sense of gratitude to my family for the support they provided me through my entire life. I am indebted to my parents for providing me the moral and emotional support. Without their kind blessings, I could not complete this work.

Apurba Kheto

CONTENTS

Contents i

List of Figures iii

List of Tables v

Synopsis vii

1 Introduction 1

1.1 General Introduction 1

1.2 Birth of a Neutron Star 2

1.3 Structure and Composition 3

1.4 Neutron Star Masses and Radius 4

1.5 Superfluidity in Neutron stars 6

2 Two Fluid Model and Relativistic Mean Field Theory 10

2.1 Fluid Formalism 10

2.2 Relativistic Mean Field Theory 13

2.3 Equilibrium Configuration 21
2.4 Calculation of Entrainment Parameter 23

3 Isospin Dependent Entrainment In Neutron Stars 26
3.1 Introduction 26
3.2 Formalism 27
3.3 Results and Discussion 38
3.4 Summary and Conclusions 47

4 Slowly Rotating Neutron Stars With Entrainment 49
4.1 Introduction 49
4.2 Methodology 50
4.2.1 Slowly rotating superfluid neutron stars 50
4.3 Results and Discussion 56
4.4 Summary and Conclusions 69

Bibliography 70

List of Figures

3.1 Neutron star sequence is plotted with central neutron density 39

3.2 Dynamical neutron and proton effective masses are shown 40

3.3 Landau effective masses are shown as a function of baryon density 41

3.4 Normalised entrainment matrix elements (Y_{ik}/Y) vs baryon density 42

3.5 Normalised entrainment matrix elements (Y_{ik}/Y) vs baryon density 43

3.6 Entrainment parameter Vs r/R in the RMF model with ρ meson 44

3.7 Entrainment parameter Vs r/R in the RMF model without ρ meson 45

3.8 Entrainment parameter in the zero velocity frame of neutrons is plotted 46

3.9 Entrainment parameter in the zero velocity frame of neutrons is plotted as . . . 47

4.1 The frame-dragging frequency $\omega(r)$ vs (r/R) 58

4.2 The metric function $v_0(r)$ is plotted as a function of radial distance 59

4.3 The metric function $m_0(r) = rv_0(r)/\exp(\lambda(r))$ is plotted 60

4.4 The metric functions $h_0(r)$ and $h_2(r)$ are plotted 61

4.5 The radial displacement $\xi_0(r)$ and $\xi_2(r)$ are plotted 62

4.6 The quantity $\bar{k}$ is plotted as a function of radial distance (r/R) 63

4.7 The rotationally induced corrections to the neutron number density 64

4.8 The rotationally induced corrections to the proton number density 64

4.9 The rotationally induced corrections to the proton number density $p_0(r)\phi_0(r)$. 65

4.10 The ratio of the polar to equatorial radii (R_p/R_e) is plotted 66

4.11 The mass-shedding (Kepler) limit is shown as a function 67

4.12 The mass-shedding (Kepler) limit is shown as a function of relative rotation rate 68

List of Tables

3.1 Nucleon-meson coupling constants in the GL and NL3 sets 38

4.1 The background nonrotating configurations for GL and NL3 sets 57

Synopsis

Neutron stars are born in the gravitational core collapse of massive stars after the supernova explosion. It contains the densest form of cold matter in the observable universe. Neutron star masses are $2M_{\odot}$ and radii are about $10 - 15$ km. Shortly after the discovery of pulsars, the study of dense matter in the core of neutron stars had gained momentum. The rapid accumulation of data on compact stars in recent years may shed light on the gross properties of cold dense matter far off normal nuclear matter density. Neutron star matter encompasses a wide range densities, from the density of iron nucleus at the surface of the star to several times normal nuclear matter density in the core. Since the chemical potentials of nucleons and leptons increase rapidly with density in the interior of neutron stars, several novel phases with large strangeness fraction such as, hyperon matter, Bose-Einstein condensates of strange mesons and quark matter may appear there. It is to be noted that strange matter typically makes the equation of state (EoS) softer resulting in a smaller maximum mass neutron star than that of the nuclear EoS. Currently the accurately measured highest neutron star mass is $2.01 \pm 0.04M_{\odot}$. This puts a strong constraint on the EoS of neutron star matter. Another interesting possibility is the presence of superfluidity in neutron star matter. Recently the fast cooling of the neutron star in Cassiopeia A (Cas A) has been observed. The rapid cooling of the neutron star in Cas A had been interpreted as the result of superfluidity in its core . It is also inferred that pulsar glitches are the manifestation of superfluid neutron matter in neutron stars. Recently, it has been argued whether the moment of inertia of the superfluid reservoir in the inner crust is sufficient to explain the latest observational data of pulsar glitches or not. When the entrainment effect which couples the neutron superfluid with the crust, is taken into account, a larger angular momentum reservoir is needed for observed glitches. Consequently, the required superfluid moment of inertia exceeds that of the superfluid crust. This indicates that the superfluid core would also contribute to pulsar glitches. Therefore, it would be worth investigating the superfluidity in neutron stars.

The fluid formalism in the case of superfluidity is different from that of the perfect fluid. For neutron stars made of neutrons, protons and electrons, two-fluid formalism was used to describe the superfluidity in neutron star matter. In this case, one fluid is the superfluid neutrons and the other fluid called the proton fluid represents the charge neutral component made of protons and electrons. It is a well known fact that two fluids in a mixture are not decoupled when one fluid interpenetrates through the other. In this situation, the momentum of one fluid is proportional to the linear combination of velocities of both fluids. This effect is known as entrainment. This effect was found in a mixture of superfluid ^{3}He and ^{4}He in the laboratory.

Neutron star matter is highly asymmetric in neutron and proton number densities. Consequently, the effects of isospin on the entrainment and superfluid dynamics in neutron stars might be important. Earlier the entrainment effect was investigated in a relativistic field theoretical model neglecting the symmetry energy and applied to the slowly rotating superfluid neutron stars. The relativistic model was inadequate to describe the neutron star matter because the σ-ω Walecka model was adopted in that calculation.

We study the entrainment effect between superfluid neutrons and charge neutral fluid (called the proton fluid) which is made of protons and electrons in neutron star interior within the two-fluid formalism and using a relativistic model where baryon-baryon interaction is mediated by the exchange of σ, ω and ρ mesons. This model of strong interaction also includes scalar self interactions. The inclusion of ρ-meson takes care of the isospin effect in neutron star matter.

The master function is calculated within a relativistic mean field (RMF) model. In this calculation, the relative motion between neutrons and protons is taken into account. Here we make the connection between the macroscopic fluid system and microscopic RMF model. In evaluating the master function as well as coefficients, the slow rotation approximation is implemented. We are dealing with superfluidity in neutron star matter which is made of neutrons, protons and electrons. When we neglect the relative motion between neutron and proton fluids, $-\Lambda|_0$ becomes the energy density of the neutron star matter. We add the contribution of electrons to the master function (Λ). Here, electrons are treated as non-interacting relativistic particles.

We consider the β-equilibrated neutron star matter to calculate the equilibrium configuration and use two different parameter sets GL and NL3 for nucleon-meson coupling constants. For the calculation of the entrainment we choose neutron star configurations which are just below maximum masses in both cases. We estimate dynamical neutron and proton effective masses for these two parameter sets. We find that the neutron effective mass increases with density and becomes greater than the free neutron mass in both cases and proton effective mass decreases with density initially and rises with density later. We also calculate the Landau effective mass for nucleons and we find that neutron and proton effective masses decrease as baryon density increases for both parameter sets, and they are below their bare masses.

We calculate the entrainment parameter for two different parameter sets. The entrainment parameter calculated using both parameter sets remains constant in the core and drops rapidly at the surface. We find an appreciable difference between the two results towards the centre. We compare this result with that of the situation excluding ρ mesons and it is clear that the inclusion of ρ mesons strongly enhances the entrainment parameter. We compare our results with those of the relativistic Landau Fermi liquid theory and find appreciable differences.

Next we explore for the first time the effects of the isospin dependent entrainment and the relative rotation between two fluids on the global properties of slowly rotating superfluid neutron stars, such as the structures and Kepler limit in the two-fluid formalism. Here we use the Hartle's slow rotation approximation to Einstein's field equation so that the equations governing rotating neutron stars in the slow rotation approximation are second order in rotational velocities of neutron and proton fluids.

We solve all sets of equations numerically using two different parameter sets (GL and NL3) and find rotationally induced corrections of different metric functions that are related to different physical quantities like mass, shape, neutron and proton number densities and Kepler frequency for realistic equations of state. First we discuss the variation of the frame-dragging frequency as a function of radial distance . The frame-dragging frequency decreases monotonically from the centre to the surface of the star for different relative rotation rates. This feature of the frame-dragging frequency is quite similar to the standard single fluid result. Further it is noted that the frame-dragging frequency is always higher for larger value of relative rotation rate.

We also solve the $l = 0$ equations and determine ξ_0, η_0, Φ_0, h_0 and v_0. Metric functions h_0 and v_0 match with the vacuum solutions at the surface. It is noted that the metric function v_0 increases monotonically to the surface and matches smoothly with the exterior solution.

For the NL3 set, the value of this metric function at the surface is always higher than that of the GL set. We solve the $\ell = 2$ equations in a similar way that is done for solutions of $\ell = 0$ equations. A new variable $\bar{k} = k_2 + h_2$ is introduced to solve two coupled first order equations in h_2 and k_2. We study the variation of h_0, h_2, ξ_o, ξ_2 and $\bar{k}$ with respect to radial distance for different rotation rates.

We explore the role of symmetry energy on the rotationally induced corrections to the proton number density by comparing two cases with and without ρ mesons for the GL set. It is noted that the corrections to the proton number density are significantly modified in the presence of ρ mesons. We also calculate the rotationally induced deformation of the star in terms of the ratio of the polar and equatorial radii. We consider the proton rotation rate to be equal to that of the fastest rotating pulsar having spin frequency 716 Hz. The non-rotating situation is achieved when the relative rotation rate approaches zero. Furthermore we find that the rotationally induced deformation of the star is larger for the NL3 case than the GL case. This deformation increases with increasing relative rotation rate.

To determine the mass shedding (Kepler) limit we have to solve the simple quadratic equation for Ω_p. When $\Omega_n > \Omega_p$ the Kepler frequency is determined by the neutrons and for $\Omega_p > \Omega_n$ the Kepler frequency is determined by the protons. We use the radial profiles of the entrainment effect in this calculation of the Kepler frequency. The results are qualitatively similar to the previous investigation by Prix and collaborators though the authors in the latter case used some constant values of entrainment. However, our results are totally different from those of Comer. When $\Omega_n/\Omega_p < 1$, the Kepler frequency (solid circles) monotonically increases with decreasing relative rotation rate whereas the opposite scenario was found in the work of Comer. It is found that the Kepler limit obtained with the isospin dependent entrainment effect is lower than that of the case when the isospin term is neglected in the entrainment effect.

We have derived the isospin dependence of the entrainment in slowly rotating superfluid neutron star in the two-fluid formalism using realistic equations of state in the Walecka model including ρ mesons and scalar self-interaction. The value of the entrainment parameter changes significantly due to the isospin effect and lies in the physical range. Next we apply this isospin dependent entrainment to study the global properties of slowly rotating neutron stars. We have shown that the Kepler limit changes due to the isospin dependent entrainment effect with respect to the case without the effects of isospin.

Our calculation on the isospin dependent entrainment may be extended to include Λ hyperons. In this case, Λ hyperons are treated as superfluid and become part of the neutron fluid in the two-fluid formalism. This might reveal the role of the core superfluid moment of inertia on pulsar glitches.

CHAPTER 1

INTRODUCTION

1.1 General Introduction

Neutron stars are the densest and compact stars in the universe. These stars are born in the gravitational core collapse of massive stars after the supernova explosion. It contains the densest form of cold matter in the observable universe. Neutron star masses are $2M_{\odot}$ [1] and radii are about $10 - 15$ km [2] and temperatures are well below 1 MeV. Neutron star matter have a wide range of densities, from the density of iron nucleus ($\rho \lesssim 10^{14} g\ cm^{-3}$) at the surface of the star to several times normal nuclear matter density ($\rho \equiv 2.7 \times 10^{14} g\ cm^{-3}$) in the core. At such high densities, various exotic forms of matter such as hyperons, quark-hadron mixed phase, Bose-Einstein condensate of kaons etc may appear. The observations of neutron stars and theoretical studies throughout past few decades could not give us a clear idea about the structure of the matter in neutron star cores and in particular its equation of state [3]. In such very high densities, neutron stars provide an exciting test platform for extreme physics [3, 4]. They are hotter,denser and have stronger magnetic fields than any other object created in the laboratory on the earth .

1.2 Birth of a Neutron Star

A typical star like our sun spends most of its luminous life (billions of years) in the hydrogen burning phase in the equilibrium state. In their cores hydrogen atoms fuse to produce helium atoms and releases large amounts of thermal energy which stabilizes the star from collapsing under the force of its own gravity. When hydrogen is exhausted in the core the star begins to collapse and increases the temperature to the point at which helium fusion starts. This Helium fusion produces large thermal energy and increases thermal pressure to stabilize the star again. For smaller stars (less than $8M_{\odot}$) the core temperature never increases enough to start fusion processes with the larger atoms. This reaction is highly temperature sensitive. This makes the star very unstable and causes a large pulsation. The whole envelope expelled into the interstellar medium due to the pulsation. The remaining carbon-oxygen core contracts under gravity but cannot attain the temperature to burn carbon. Now the gravity is balanced by the electron degeneracy pressure and the star gradually cools down to form a white dwarf. For a larger star (grater than $8M_{\odot}$) the fusion process continues and the atoms combine until they are producing iron(Fe^{56}) because this is the largest atom for which the fusion produces energy. As there is no burning and therefore no outward thermal pressure in the core; it begins to collapse under gravity. Material from shell burning deposits to the stars core and when it exceed the Chandrasekhar limit, the electron degeneracy pressure cannot balance the gravity and the core continues to collapse. The rapidly collapsing core creates heat and starts photo disintegration of iron nuclei into helium nuclei and free neutrons. Then the core density increases and producing neutrons and neutrinos via the inverse beta decay process. Neutrinos produced in this process weakly interact with matter and escape from the core carrying away energy and further accelerating the collapse. When core density further increases the neutrino diffusion time scale is larger than the collapsing time scale and they get trapped inside the core. When the density inside the core exceeds the nuclear density ($10^{14} g\ cm^{-3}$) then nuclei dissolve to form nuclear matter. The short-range repulsion of nucleons together with the degeneracy pressure of nucleons resists further collapse and generates a shock wave. This shock has sufficient energy to expel the whole steller envelope. This event is called the supernova explosion. If the initial mass of the star is less than $20M_{\odot}$, the remnant might form a neutron star. In a neutron star the force of gravity is balanced by the neutron degeneracy pressure.

1.3 Structure and Composition

Neutron stars have several regions like the inner and outer cores, the crust, the envelope and the atmosphere. The atmosphere with thickness of a few centimeters contains plasma of H, He and possibly a trace of heavier elements that contribute to a negligible amount of mass and plays an important role in shaping the electromagnetic spectrum. Just below the atmosphere there is a thin envelope which is a few meter thick and influences the transport and release of thermal energy from the stars surface. The outer crust is made of nuclei and free electrons. Outer crust begins at $\rho \sim 10^4 g\ cm^{-3}$. Above density $4 \times 10^{11} g\ cm^{-3}$ the chemical potential of neutrons becomes equal to the bare neutron mass. So that neutrons leak out from nuclei. This point is called the neutron drip point and it marks the end of the outer crust and the beginning of the inner crust. The inner crust is composed of nuclei, free neutrons and electrons. With increasing density, number of dripped neutrons as well as the volume fraction occupied by the nuclei increases. When volume fraction becomes larger, it may become energetically favorable for the nuclei to undergo a series of transitions from spherical shape to cylinder, slab, cylindrical bubble and spherical bubble with increasing density. This phase is known as the nuclear pasta [5, 6].

The core constitutes up to ninety-nine percentage of the mass of the star. The outer core consists of a soup of nucleons, electrons and muons. The neutrons could form a ${}^3P_2$ superfluid and the protons a ${}^1S_0$ superconductor within the outer core. In the inner core various exotic forms of matter such as hyperons, quark-hadron mixed phase, Bose-Einstein condensate of kaons etc may appear.

1.4 Neutron Star Masses and Radius

The structure of neutron stars depends on the relation between energy density and pressure in the interior of neutron stars i.e equation of state (EoS). Since it is not possible to create such extreme density in laboratory experiments, so the physical properties of such matter in this extremely high density can only be studied on the basis of some theoretical model [7]. For a soft EOS the maximum mass will be low and a stiff EoS produces larger maximum mass. Understanding the EoS of matter at supranuclear densities it is important to measure neutron-star masses. The mass of a neutron star is accurately measured if it is in a binary system. The most accurate masses have been derived from timing studies for the binary radio pulsars and all of these were consistent with a small mass range near $1.35M_\odot$ [8]. These radio pulsars are orbiting another neutron star, a white dwarf or a main-sequence star. The observations of pulsars in binaries yield orbital sizes and periods from Doppler shift phenomenon, from which the total mass of the system can be obtained. To know the individual mass of these compact binary system it is necessary to constrain the orbital parameters such as inclination angle, period, semi-major axis etc. The compact nature of binary pulsars allows detection of some relativistic effects such as Shapiro delay [9], periastron advance, gravitational redshift and orbit shrinkage due to gravitational waves, which constrains the inclination angle. A well observed system like the binary pulsar PSR 1913+16 [10] or the newly discovered double pulsar binary PSR J0737-3039 [11], masses of these pulsers have been determined to impressive accuracy. Masses can be measured for neutron stars that are accreting matter from a stellar companion in x-ray binaries. Due to the difficulties in determination of parameters of orbital motion in the binary system and some uncertain interfering factors these measurements have large uncertainties. Direct mass estimates have been obtained for several X-ray pulsars like 4U 1700-37, Vela X-1 and pulsar J0751+1807 with large relative error. The mass obtained for Vela X-1 pulsar is quite high ($2M_{\odot}$) with large error. The estimated mass of the x-ray binary 4U1700+37 is $2.44 \pm 0.27 M_{\odot}$. Raising the limit for the neutron star maximum mass could eliminate entire EOS families, especially those in which exotica appear. It is to be noted that the strange matter typically makes the equation of state (EoS) softer resulting in a smaller maximum mass neutron star than that of the nuclear EoS [4]. Currently the accurately measured highest neutron star mass is $2.01 \pm 0.04 M_{\odot}$ [1]. This puts a strong constraint on the EoS of neutron star matter.

Neutron stars are situated at very large distances from the earth. So the accurate measurements of radii of such high distanced object are very challenging because there are no direct methods for the determination of the radius. But there exists some indirect methods by which one can try to measure the radius of a neutrons star. In one such approach the radius of a neutron star is measured by analyzing the thermal spectrum emitted from its surface. Radius estimates from isolated neutron stars are affected by various facts like distance uncertainties, non uniformity of steller temperature and absorption in steller surface. The radiation spectrum deviates from that of a ideal blackbody radiation. The isolated pulsars like Geminga, RX J18563.5-3754 and PSR B0656+14, distances have been obtained by the parallax method with appreciable errors. The recent discovery of thermal radiation from quiescent x-ray bursters in globular clusters is particularly exciting. It is believed the billion years old neutron stars in globular clusters could be hot enough to emit observable thermal radiation. The measurements of radii from these stars might become relatively acurate when the distances to the globular clusters in which they are found can be refined. Absorption lines in X-ray spectra have also been suggested for deducing neutron star radius. Accurate measurement of a neutron star radius would constrain the dense matter EoS. Various structural quantities that are relatively EoS independent like the moment of inertia and binding energy could be used to constrain the neutron star mass-radius relationship.

1.5 Superfluidity in Neutron stars

After the formation, neutron stars cool down by the emission of neutrino anti-neutrino pairs in the neutrino cooling era. When the temperature inside the neutron star drops sufficiently nucleons might form pairs. The idea of superfluidity inside neutron stars was first proposed by Migdal [12]. The implications of neucleonic pairing in neutron star matter were explored by G. Baym et. al [13]. Soon after the discovery of pulsars, microscopic calculations of nucleonic pairing gaps was studied by various groups [14–18]. In a sufficiently cold and dense fermionic matter, an attractive interaction at the Fermi surface leads to the formation of cooper pairs. In the inner crust, neutron superfluidity is produced by Cooper pairing via the attractive singlet $^1S_0$ channel. Superfluidity occurs when the temperature inside the stars falls below the critical temperature. The critical temperature which is a function of density depends on the model of nucleon-nucleon interaction. [19].

The formation of neutron superfluidity and proton superconductivity in neutron star cores are predicted by many microscopic theories [19, 20]. These are produced by the nn and pp Cooper pairing due to the attractive interaction in the Fermi surface. This superfluidity and superconductivity are characterized by the respective critical temperatures T_{cn} and T_{cp}. As the density increases towards the core, the strong short range repulsive interaction comes into play and due to this repulsive interaction the pairing effect is quenched [21]. In the density regime $(10^{14} g\ cm^{-3})$ the crust nuclei dissolve into a quantum liquid of neutrons and protons. In the interior of the quantum fluid, ${}^1S_0$ proton pairing occurs. The neutron superfluidity may also apper in the coupled ${}^3P_2 - {}^3F_2$ two neutron channel [20, 22]. Superfluidity from other baryons such as hyperons may be also possible. Neutron, proton and possible hyperon superfluidity in the ${}^1S_0$ channel, and neutron superfluidity in the ${}^3P_2$ channel have been predicted with gaps of a few MeV [23].

Neutron superfluidity and proton superconductivity in neutron stars have a number of interesting consequences for thermal evolution and observed spin behavior. Recently rapid cooling of Cassiopeia A has been reported [24–28]. As the neutron star cools, its temperature will drop below critical temperature for the onset of superfluid, the neutrino emission channel is opened up and the cooling of the neutron star is speeded up. It was proposed that the observed rapid cooling of the neutron star in Cassiopeia A was due to the enhanced neutrino emission from the recent onset of the breaking and formation of neutron Cooper pairs in the ${}^3P_2$ channel and the specific heat of the stellar interior which is determined by the state of the matter, while neutrino emission processes which cool a young neutron star are strongly suppressed in the presence of hadronic superfluids. The rapid cooling of this neutron star had been interpreted as the result of superfluidity in its core. This is the first direct evidence that the superfluidity or superconductivity occurs at supranuclear density in a neutron star [25–28].

Glitches is the phenomenon in which pulsars jumps in spin rate. Interaction of superfluid vorticity with the nuclei of the inner crust or superconducting flux tubes in the core could lead to the glitches seen in many neutron stars [29]. It is also inferred that pulsar glitches are the manifestation of superfluid neutron matter in neutron stars [30–33]. This glitch phenomenon might be described based on the pinning and unpinning of superfluid quantized vortices in neutron stars. Recently, it has been argued whether the moment of inertia of the superfluid reservoir in the inner crust is sufficient to explain the latest observational data of pulsar glitches or not [30, 31]. When the entrainment effect which couples the neutron superfluid with the crust, is taken into account, a larger angular momentum reservoir is needed for observed glitches [30]. Consequently, the required superfluid moment of inertia exceeds that of the superfluid crust. This indicates that the superfluid core would also contribute to pulsar glitches.

Entrainment is also an important phenomenon occurred inside the superfluid neutron stars where we consider one fluid is the neutron superfluid and other fluid is the proton fluid. When two fluids flow parallelly the momentum of one fluid is proportional to the linear combination of velocities of both fluids. This effect is known as the entrainment. The notion of the entrainment in the theory of mixtures of two superfluid ^{3}He and ^{4}He was first introduced by Andreev and Bashkin [34]. The entrainment effect was applied in npe phase of superfluid neutron stars to study the dependence of the generated magnetic moment of the star on the strength of the proton drag currents produced by the neutrons [35]. The entrainment effect inside the superfluid neutron star has been studied intensively in understanding rotational equilibria, oscillations of superfluid neutron stars [36–39] and the pulsar glitch [30, 31]. In this thesis we basically describe the isospin dependence of the entrainment effect inside the superfluid neutron star including ρ mesons that is responsible for the symmetry energy in the relativistic mean field theory. We also explore for the first time the effects of the isospin dependent entrainment and the relative rotation between two fluids on the global properties of slowly rotating superfluid neutron stars, such as the structures and Kepler limit in the two-fluid formalism.

We organise this thesis in the following way. We describe the fluid formalism i.e two fluid model in connection with superfluid neutron stars, the relativistic $\sigma - \omega - \rho$ model for the entrainment and the definition of entrainment parameter in Chapter 2. In Chapter 3 we describe the isospin dependence of the entrainment effect and its radial profile inside the stars [40]. The different dynamical parameters of a slowly rotating stars in the presence of the isospin dependent entrainment are discussed in Chapter 4.

CHAPTER 2

TWO FLUID MODEL AND RELATIVISTIC MEAN FIELD THEORY

2.1 Fluid Formalism

Here we discuss the two fluid formalism that is originally developed by Carter and his collaborators [41–47] to describe the fluid motion inside the superfluid neutron stars. The details of this superfluid formalism is described by Anderson [48]. They construct an action principle to yield the equations of motion and the stress-energy tensor. Here we only consider the two fluids - one component is the neutron fluid and the other is the proton fluid. The central quantity of the superfluid dynamics is the "master" function Λ. It depends on the three scalar $n^2 = -n_\mu n^\mu$, $p^2 = -p_\mu p^\mu$ and $x^2 = -n_\mu p^\mu$ where n^μ and p^μ are the conserved neutron and proton current densities.

In the limit when all the currents are parallel, $-\Lambda$ corresponds again to the local thermodynamic energy density. In the action principle, Λ is the Lagrangian density for the fluids. The fluid currents forming scalars imply that the system is locally isotropic in the sense that the fluids are equally free to move in any direction.

An unconstrained variation of the master function Λ with respect to the independent vectors n^{μ},p^{μ} and the metric $g_{\mu\nu}$ takes the form [48]

$$\delta\Lambda = \sum_{\mathrm{x}=\{n,p\}} \mu^{n}_{\mu}\delta \mathrm{x}_{\mathrm{x}}\mathrm{x}^{\mu} + \frac{1}{2}g^{\lambda\nu}\left(\sum_{\mathrm{x}=\{n,p\}} \mathrm{x}^{\mu}_{\mathrm{x}}\mu^{\mathrm{x}}_{\lambda}\right)\delta g_{\mu\nu} \ , \tag{2.1}$$

where

$$\mu^{n}_{\mu} = g_{\mu\nu}\left(\mathcal{B}n^{\nu} + \mathcal{A}p^{\nu}\right) = \mu_{\mu} \ , \tag{2.2}$$

$$\mu^{p}_{\mu} = g_{\mu\nu}\left(\mathcal{A}n^{\nu} + \mathcal{C}p^{\nu}\right) = \chi_{\mu} \ , \tag{2.3}$$

$$\mathcal{A} = -\frac{\partial\Lambda}{\partial x^2} \ , \mathcal{B} = -2\frac{\partial\Lambda}{\partial n^2} \ , \mathcal{C} = -2\frac{\partial\Lambda}{\partial p^2} \ . \tag{2.4}$$

The momentum covectors μ_{μ} and χ_{μ} are dynamically, and thermodynamically, conjugate to their respective number density currents n^{μ} and p^{μ}, and their magnitudes are the chemical potentials. From the above two equations (2.2) and (2.3), it is clear that the momentum of one constituent carries along some mass current of the other constituents. The current and momentum for a particular fluid do not have to be parallel. This effect is known as the entrainment effect. The entrainment only vanishes in the special case where Λ is independent of x^2.

Now the variation of master function in terms of the constrained Lagrangian displacements gives [48]

$$\delta\left(\sqrt{-g}\Lambda\right) \ = \ \frac{1}{2}\sqrt{-g}\left(\Psi\delta^{\mu}{}_{\lambda} + \sum_{\mathrm{x}=\{n,p\}} n^{\mu}_{\mathrm{x}}\mu^{\mathrm{x}}_{\lambda}\right) g^{\lambda\nu}\delta g_{\mu\nu} - \sqrt{-g}\sum_{\mathrm{x}=\{n,p\}} f^{\mathrm{x}}_{\nu}\xi^{\nu}_{\mathrm{x}}$$

$$+\nabla_\nu \left(\frac{1}{2}\sqrt{-g} \sum_{\mathrm{x}=\{n,p\}} \mu_{\mathrm{x}}^{\nu\lambda\tau} n^{\mathrm{x}}_{\lambda\tau\mu} \xi^\mu_{\mathrm{x}} \right) , \tag{2.5}$$

where

$$f^{\mathrm{x}}_\nu = 2n^\mu_{\mathrm{x}} \omega^{\mathrm{x}}_{\mu\nu} , \tag{2.6}$$

and

$$\omega^{\mathrm{x}}_{\mu\nu} = \nabla_{[\mu} \mu^{\mathrm{x}}_{\nu]} . \tag{2.7}$$

The generalized pressure Ψ is now

$$\Psi = \Lambda - n^\rho \mu_\rho - p^\rho \chi_\rho . \tag{2.8}$$

Here it is clear that n^μ and p^μ are the fundamental variables for the fluids. The equations of motion consist of the two original conservation conditions plus two Euler type equations.

The stress-energy tensor is given by

$$T^\mu_\nu = \Psi \delta^\mu_\nu + n^\mu \mu_\nu + p^\mu \chi_\nu \tag{2.9}$$

The averaged stress energy tensors which are the basic input of the Einstein equations are calculated from the fluid hydrodynamics. In the next section 2.2, we discuss about the relativistic mean field theory to relate fluid stress energy tensors to matter stress energy tensors.

2.2 Relativistic Mean Field Theory

Walecka [49] introduced a field-theoretical model motivated by the experimental observation of large Lorentz scalar and four-vector components of self energies in the NN interaction. This model is also known as the $\sigma - \omega$ model. This is used to describe the properties of nuclei as well as nuclear matter. In the model , the interaction between nucleons arises from the exchange of two massive mesons: the scalar meson σ with mass m_σ the vector meson ω_μ with mass m_ω. But this $\sigma-\omega$ model was unable to reproduce the empirical value of the incompressibility, the effective nucleon mass and the symmetry energy at the saturation density of nuclear matter. To solve this problem, Boguta and Bodmer [50] introduced non-linear self-interactions of the scalar meson (σ) in this model. The model was further extended by including a vector-isovector meson (ρ) which accounts for the symmetry energy of the nuclear matter. Throughout this thesis, we use the Misner-Throne-Wheeler [51] metric conventions. In a static neutron star matter the relativistic mean field theory is very useful to describe the microphysics of the dense nuclear matter. The Lagrangian density for nucleon-nucleon interaction is given by [4]

$$\begin{aligned}\mathcal{L}_B &= \sum_{B=n,p} \bar{\Psi}_B \left(i\gamma_\mu \partial^\mu - m_B + g_{\sigma B}\sigma - g_{\omega B}\gamma_\mu \omega^\mu - g_{\rho B}\gamma_\mu \mathrm{t}_B \cdot \boldsymbol{\rho}^\mu\right) \Psi_B \\ & -\frac{1}{2}\left(\partial_\mu \sigma \partial^\mu \sigma + m_\sigma^2 \sigma^2\right) - U(\sigma) \\ & -\frac{1}{4}\omega_{\mu\nu}\omega^{\mu\nu} - \frac{1}{2}m_\omega^2 \omega_\mu \omega^\mu - \frac{1}{4}\boldsymbol{\rho}_{\mu\nu} \cdot \boldsymbol{\rho}^{\mu\nu} - \frac{1}{2}m_\rho^2 \boldsymbol{\rho}_\mu \cdot \boldsymbol{\rho}^\mu \,. \end{aligned} \tag{2.10}$$

Here ψ_B denotes the Dirac bispinor for baryons B with vacuum mass m_B and the isospin operator is t_B. The scalar self-interaction term [50] is $U(\sigma) = \frac{1}{3}bm\left(g_\sigma \sigma\right)^3 + \frac{1}{4}c\left(g_\sigma \sigma\right)^4$. Equations of motion for the fields are obtained from the Euler-Lagrange equation

$$\partial_\mu \frac{\partial \mathcal{L}}{\partial(\partial_\mu \phi)} = \frac{\partial \mathcal{L}}{\partial \phi} \tag{2.11}$$

where ϕ represents the fields σ, ω, ρ and ψ. Now using the equations (2.10) and (2.11) we get the following equations

$$\left(-\Box + m_\sigma^2\right)\sigma = \sum_{B=n,p} g_\sigma \bar{\Psi}_B \Psi_B - bm{g_\sigma}^3\sigma^2 - c{g_\sigma}^4\sigma^3\,, \tag{2.12}$$

$$\left(-\Box + m_\omega^2\right)\omega_\mu + \partial_\mu\partial^\nu\omega_\nu = -\sum_{B=n,p} g_\omega \bar{\Psi}_B \gamma_\mu \Psi_B, \tag{2.13}$$

$$\left(-\Box + m_\rho^2\right)\rho_\mu + \partial_\mu\partial^\nu\rho_\nu = -\sum_{B=n,p} \frac{1}{2} g_\rho \tau . \bar{\Psi}_B \gamma_\mu \Psi_B, \tag{2.14}$$

$$\sum_{B=n,p}(i\gamma_\mu\partial^\mu - m)\Psi_B = \sum_{B=n,p}(g_\omega\gamma_\mu\omega^\mu - g_\sigma\sigma + \frac{1}{2}g_\rho\rho^\mu.\tau\bar{\psi}\gamma_\mu)\Psi_B\,. \tag{2.15}$$

Equations (2.12)- (2.15) form a set of coupled nonlinear differential equations. Exact solutions of the above equations are very difficult. We can use the mean-filed approximation to study the dense and uniform matter of neutron stars where the meson field operators are replaced by their ground state expectation values as

$$\sigma \rightarrow <\sigma>,$$

$$\omega_\mu \rightarrow <\omega_\mu>,$$

$$\rho_\mu \rightarrow <\rho_\mu>.$$

Now we set the mean field equation to the fluid motion inside the neutron star. Here we choose a frame in which neutrons have zero spatial momentum and protons have a wave vector $k_\mu = (k_0, 0, 0, k)$. The Dirac nucleon effective mass m_* is defined as $m_* = m- < g_\sigma \sigma >$. The first two components of the isovector field (ρ) also have vanishing expectation values in the ground state so that only the third component survives. Here we use the nucleon mass (m) which is the average of bare neutron (m_n) and proton (m_p) masses. Applying the mean field approximation and neglecting all the derivative terms, finally we get from equations (2.12)-(2.15)

$$m_* = m - c_\sigma^2 \sum_{B=n,p} < \bar{\Psi}_B \Psi_B > \tag{2.16}$$

$$< g_\omega \omega_\mu >= - \sum_{B=n,p} c_\omega^2 < \bar{\Psi}_B \gamma_\mu \Psi_B > \tag{2.17}$$

$$< g_\rho \rho_\mu^3 >= -\frac{1}{2} c_\rho^2 \sum_{B=n,p} < \bar{\Psi}_B \tau_3 \gamma_\mu \Psi_B > . \tag{2.18}$$

where $c_\sigma^2 = (g_\sigma/m_\sigma)^2$, $c_\omega^2 = (g_\omega/m_\omega)^2$ and $c_\rho^2 = (g_\rho/m_\rho)^2$.

In the zero-momentum frame of the neutrons , we get algebraic equations of ω_μ and ρ_μ fields. The time and spatial components of the vector mesons are given by

$$< g_\omega \omega_0 >= -c_\omega^2 \sum_{B=n,p} < \bar{\Psi}_B \gamma_0 \Psi_B >, \tag{2.19}$$

$$< g_\omega \omega_z >= -c_\omega^2 \sum_{B=n,p} < \bar{\Psi}_B \gamma_z \Psi_B >, \tag{2.20}$$

$$< g_\rho \rho_0^3 >= -\frac{1}{2} c_\rho^2 \sum_{B=n,p} < \bar{\Psi}_B \tau_3 \gamma_0 \Psi_B >, \tag{2.21}$$

$$< g_\rho \rho_z^3 >= -\frac{1}{2} c_\rho^2 \sum_{B=n,p} < \bar{\Psi}_B \tau_3 \gamma_z \Psi_B > . \tag{2.22}$$

The right hand side (r.h.s) of equations (2.20) and (2.22) vanishes by isotropy if the ground state of the neutron star matter is static or neutrons and protons have an average zero momentum. But here we are interested to calculate the expectation values of the mesons field in the medium where neutrons and protons have a relative velocity. So there is a flow of neutrons and protons along the z-axis and the problem is that we can not define a common rest frame of neutrons and protons. The r.h.s of these equations involves an integration over a Fermi sphere of the particle. Here we choose the proton Fermi surface is displaced by an amount $k_z\hat{z}$. Now the Dirac equation

$$< \bar{\Psi}_B[\gamma^\mu(i\partial_\mu - g_\omega\omega_\mu - \frac{1}{2}g_\rho\tau_3\rho^3_\mu) - (m - g_\sigma\sigma)]\Psi_B >= 0, \tag{2.23}$$

can be written in following form

$$(k^0 + g_\omega\omega^0 + \frac{1}{2}g_\rho\tau_3\rho^0_3)^2 = (\vec{k} + g_\omega\omega^z\hat{z} + \frac{1}{2}g_\rho\tau_3\rho^z_3\hat{z})^2 + m^2_*. \tag{2.24}$$

So the energy of a baryon in a plane wave state is given by the above equation

$$\epsilon(\overrightarrow{k}) = E(\overrightarrow{k}) - g_\omega\omega_0 - \frac{1}{2}g_\rho\tau_3\rho^0_3 = \sqrt{(\overrightarrow{k} + g_\omega\omega^z\hat{z} + \frac{1}{2}g_\rho\tau_3\rho^z_3\hat{z})^2 + m^2_*} - g_\omega\omega_0 - \frac{1}{2}g_\rho\tau_3\rho^0_3. \tag{2.25}$$

Here we see that ω_0 and ρ^0_3 give a constant shift of the energy , ω_z and ρ^z_3 give the preferred frame of momenta and σ renormalizes the Dirac mass. Due to the presence of rho meson the degeneracy of nucleons is removed. Now the expectation values are calculated in the following way. The scalar density is given by [4]

$$\langle \bar{\Psi_B}\Psi_B \rangle = \frac{1}{(2\pi)^3}\int_{occ} d^3k\,\frac{\partial E}{\partial m},$$

$$
\begin{aligned}
&= \frac{2}{(2\pi)^3}\int_{|\vec{k}|<k_n} d^3k\,\frac{m_*}{\sqrt{(\vec{k}+g_\omega\omega_z\widehat{z}-\frac{1}{2}g_\rho\rho_3^z\widehat{z})^2+m_*^2}} \\
&\quad+\frac{2}{(2\pi)^3}\int_{|\vec{k}-K\widehat{z}|<k_p} d^3k\,\frac{m_*}{\sqrt{(\vec{k}+g_\omega\omega_z\widehat{z}+\frac{1}{2}g_\rho\rho_3^z\widehat{z})^2+m_*^2}}, \\
&= \frac{2}{(2\pi)^3}\int_{|\vec{k}|<k_n} d^3k\,\frac{m_*}{\sqrt{(\vec{k}+g_\omega\omega_z\widehat{z}-\frac{1}{2}g_\rho\rho_3^z\widehat{z})^2+m_*^2}} \\
&\quad+\frac{2}{(2\pi)^3}\int_{|\vec{k}|<k_p} d^3k\,\frac{m_*}{\sqrt{(\vec{k}+g_\omega\omega_z\widehat{z}+\frac{1}{2}g_\rho\rho_3^z\widehat{z}+K\widehat{z})^2+m_*^2}}\,. \qquad (2.26)
\end{aligned}
$$

Similarly, we calculate the average four velocity component of baryons [4]

$$
\begin{aligned}
\left\langle \bar{\Psi}_B\gamma^0\Psi_B\right\rangle &= \frac{2}{(2\pi)^3}\int_{|\vec{k}|<k_n} d^3k\,+\frac{2}{(2\pi)^3}\int_{|\vec{k}|<k_p} d^3k, \\
\left\langle \bar{\Psi}_B\gamma^z\Psi_B\right\rangle &= \frac{2}{(2\pi)^3}\int_{|\vec{k}|<k_n} d^3k\frac{k^z+g_\omega\omega^z-\frac{1}{2}g_\rho\rho_3^z}{\sqrt{(\vec{k}+g_\omega\omega^z\widehat{z}-\frac{1}{2}g_\rho\rho_3^z\widehat{z})^2+m_*)^2}} \\
&\quad+\frac{2}{(2\pi)^3}\int_{|\vec{k}|<k_p} d^3k\frac{k^z+g_\omega\omega^z+\frac{1}{2}g_\rho\rho_3^z+K}{\sqrt{(\vec{k}+g_\omega\omega^z\widehat{z}+\frac{1}{2}g_\rho\rho_3^z\widehat{z}+K\widehat{z})^2+m_*^2}}. \qquad (2.27)
\end{aligned}
$$

The stress-energy tensor is defined as

$$
T^{\mu\nu}=\frac{\partial\mathcal{L}}{\partial(\partial_\mu\phi)}\partial^\nu\phi-\eta^{\mu\nu}\mathcal{L}. \qquad (2.28)
$$

Using the above definition (2.28) and the Lagrangian density given by (2.10), we calculate the stress-energy tensor containing contributions from baryons (b), mesons (σ,ω,ρ), and their interactions

$$
T^{\mu\nu}=T_b^{\mu\nu}+T_\sigma^{\mu\nu}+T_\omega^{\mu\nu}+T_\rho^{\mu\nu}+T_{int}^{\mu\nu}. \qquad (2.29)
$$

$$
\begin{aligned}
T^{\mu\nu} &= -\sum_{B=n,p} i\bar{\Psi_B}(\gamma^\mu\partial^\nu - \eta^{\mu\nu}\gamma^\alpha\partial_\alpha)\Psi_B - \sum_{B=n,p} m\eta^{\mu\nu}\bar{\Psi_B}\Psi_B + \partial^\mu\sigma\partial^\nu\sigma - \frac{1}{2}\eta^{\mu\nu}m_\sigma^2\sigma^2 \\
&\quad -\frac{1}{2}\eta^{\mu\nu}\partial^\alpha\sigma\partial_\alpha\sigma - \frac{1}{3}\eta^{\mu\nu}bm\left(g_\sigma\sigma\right)^3 - \frac{1}{4}\eta^{\mu\nu}c\left(g_\sigma\sigma\right)^4 \\
&\quad +\left(\partial^\mu\omega^\alpha - \partial^\alpha\omega^\mu\right)\partial^\nu\omega_\alpha - \frac{1}{2}\eta^{\mu\nu}m_\omega^2\omega^\alpha\omega_\alpha - \frac{1}{4}\eta^{\mu\nu}m_\omega^2\omega^{\alpha\beta}\omega_{\alpha\beta} + \left(\partial^\mu\rho^\alpha - \partial^\alpha\rho^\mu\right)\partial^\nu\rho_\alpha \\
&\quad -\frac{1}{2}\eta^{\mu\nu}m_\rho^2\rho^\alpha\rho_\alpha - \frac{1}{4}\eta^{\mu\nu}m_\rho^2\rho^{\alpha\beta}\rho_{\alpha\beta} + \eta^{\mu\nu}\sum_{B=n,p} g_\sigma\sigma\bar{\Psi_B}\Psi_B \\
&\quad -\eta^{\mu\nu}\sum_{B=n,p} g_\omega\omega_\alpha\bar{\Psi_B}\gamma^\alpha\Psi_B - \eta^{\mu\nu}\sum_{B=n,p} g_\rho\rho_\alpha.\tau\bar{\Psi_B}\gamma^\alpha\Psi_B
\end{aligned} \tag{2.30}
$$

Using equations (2.16)- (2.18) we get the final form of the averaged stress energy tensor from equation (2.30)

$$
\begin{aligned}
< T_\mu^\nu > &= -\frac{1}{2}(c_\omega^{-2} < g_\omega\omega^\alpha >< g_\omega\omega_\alpha > + c_\rho^{-2} < g_\rho\rho^\alpha >< g_\rho\rho_\alpha > + c_\sigma^{-2}[m - m_*]^2)\delta_\nu^\mu \\
&\quad -i\sum_{B=n,p} < \bar{\Psi}_B\gamma^\mu\partial_\nu\Psi_B > + \frac{2}{3}bm\left(g_\sigma\sigma\right)^3 + \frac{1}{2}c\left(g_\sigma\sigma\right)^4 .
\end{aligned} \tag{2.31}
$$

The stress-energy tensor is the input for the Einstein equations. In the zero momentum frame of neutrons, the averaged stress-energy tensor components are obtained by using equation (2.31),

$$
\begin{aligned}
\left\langle T_0^0\right\rangle &= -\frac{1}{2}c_\omega^2\sum_{B=n,p}\left(\left\langle\bar{\psi}_B\gamma^0\psi_B\right\rangle^2 - \left\langle\bar{\psi}_B\gamma^z\psi_B\right\rangle^2\right) \\
&\quad -\frac{1}{2}c_\rho^2\sum_{B=n,p}\left(\left\langle\bar{\psi}_B I_{3B}\gamma^0\psi_B\right\rangle^2 - \left\langle\bar{\psi}_B I_{3B}\gamma^z\psi_B\right\rangle^2\right) \\
&\quad -\frac{1}{2}c_\sigma^{-2}\left(m^2 - m_*^2\right) - \frac{1}{3}bm\left(m - m_*\right)^3 \\
&\quad -\frac{1}{4}c\left(m - m_*\right)^4 - \sum_{B=n,p}\left\langle\bar{\psi}_B\gamma^i k_i\psi_B\right\rangle ,
\end{aligned} \tag{2.32}
$$

$$\left\langle T_z^0 \right\rangle = \sum_{B=n,p} \left\langle \bar{\psi}_B \gamma^0 k_z \psi_B \right\rangle \tag{2.33}$$

$$\begin{aligned}\left\langle T_x^x \right\rangle &= \left\langle T_y^y \right\rangle = \frac{1}{2} c_\omega^2 \sum_{B=n,p} \left(\left\langle \bar{\psi}_B \gamma^0 \psi_B \right\rangle^2 - \left\langle \bar{\psi}_B \gamma^z \psi_B \right\rangle^2 \right) \\ &+ \frac{1}{2} c_\rho^2 \sum_{B=n,p} \left(\left\langle \bar{\psi}_B I_{3B} \gamma^0 \psi_B \right\rangle^2 - \left\langle \bar{\psi}_B I_{3B} \gamma^z \psi_B \right\rangle^2 \right) \\ &- \frac{1}{2} c_\sigma^{-2} (m - m_*)^2 - \frac{1}{3} bm (m - m_*)^3 \\ &- \frac{1}{4} c (m - m_*)^4 + \sum_{B=n,p} \left\langle \bar{\psi}_B \gamma^x k_x \psi_B \right\rangle \ , \end{aligned} \tag{2.34}$$

$$\begin{aligned}\left\langle T_z^z \right\rangle &= \frac{1}{2} c_\omega^2 \sum_{B=n,p} \left(\left\langle \bar{\psi}_B \gamma^0 \psi_B \right\rangle^2 - \left\langle \bar{\psi}_B \gamma^z \psi_B \right\rangle^2 \right) \\ &+ \frac{1}{2} c_\rho^2 \sum_{B=n,p} \left(\left\langle \bar{\psi}_B I_{3B} \gamma^0 \psi_B \right\rangle^2 - \left\langle \bar{\psi}_B I_{3B} \gamma^z \psi_B \right\rangle^2 \right) \\ &- \frac{1}{2} c_\sigma^{-2} (m - m_*)^2 - \frac{1}{3} bm (m - m_*)^3 \\ &- \frac{1}{4} c (m - m_*)^4 + \sum_{B=n,p} \left\langle \bar{\psi}_B \gamma^z k_z \psi_B \right\rangle \ , \end{aligned} \tag{2.35}$$

where I_{3B} is the third isospin component for baryon B. Averaged stress-energy tensor components include terms which are to be integrated over neutron and proton Fermi surfaces but now in terms of completely known parameters. To determine $\langle T_z^z \rangle$, we have to calculate

$$\begin{aligned}\sum_{B=n,p} \left\langle \bar{\Psi_B} \gamma^z k_z \Psi_B \right\rangle &= \frac{2}{(2\pi)^3} \int_{|\vec{k}|<k_n} d^3k \ k^z \frac{\partial E}{\partial k^z} + \frac{2}{(2\pi)^3} \int_{|\vec{k}-K\widehat{z}|<k_p} d^3k \, k^z \frac{\partial E}{\partial k^z} \\ &= \frac{2}{(2\pi)^3} \int_{|\vec{k}|<k_n} d^3k \ k_z \left[k_z + g_\omega \omega_z - \frac{1}{2} g_\rho \rho_3^z \right] \times \\ &\left[\left(\vec{k} + g_\omega \omega^z \widehat{z} - \frac{1}{2} g_\rho \rho_3^z \widehat{z} \right)^2 + m_*^2 \right]^{-1/2} \end{aligned}$$

$$+\frac{2}{(2\pi)^3}\int_{|\vec{k}|<k_p} d^3k\ \ [k_z+K]\left[k_z+g_\omega\omega_z+\frac{1}{2}g_\rho\rho_3^z+K\right]\times$$
$$\left[\left(\vec{k}+g_\omega\omega^z\widehat{z}+\frac{1}{2}g_\rho\rho_3^z\widehat{z}+K\widehat{z}\right)^2+m_*^2\right]^{-1/2}, \tag{2.36}$$

and for $\langle T_z^0\rangle$

$$\sum_{B=n,p}\left\langle\bar{\Psi_B}\gamma^0 k_z\Psi_B\right\rangle=\frac{2}{(2\pi)^3}\int_{|\vec{k}|<k_n} d^3k\ k_z+\frac{2}{(2\pi)^3}\int_{|\vec{k}|<k_p} d^3k\ (k_z+K)=\frac{k_p^3}{3\pi^2}K\ . \tag{2.37}$$

We use the equations(2.16) and (2.26) and perform integrations in cylindrical coordinates with the definitions $\phi_\omega=g_\omega\omega^z$,$\phi_{\omega K}=\phi_\omega+K$ and $\phi_\rho=g_\rho\rho_3^z$ as in Ref. [52]. We write the effective mass explicitly as [40],

$$\begin{aligned}m_* &= m-\frac{c_\sigma^2}{2\pi^2}m_*\left(\int_{-k_n}^{k_n}dk_z\left[k_n^2+\phi_\omega^2+\frac{1}{4}\phi_\rho^2+m_*^2+2\phi_\omega k_z-\phi_\rho k_z-\phi_\omega\phi_\rho\right]^{1/2}\right.\\ &+\int_{-k_p}^{k_p}dk_z\left[k_p^2+\left(\phi_{\omega K}+\frac{1}{2}\phi_\rho\right)^2+m_*^2+2\left(\phi_{\omega K}+\frac{1}{2}\phi_\rho\right)k_z\right]^{1/2}\\ &\left.-\int_{-k_n}^{k_n}dk_z\left[\left(k_z+\phi_\omega-\frac{1}{2}\phi_\rho\right)^2+m_*^2\right]^{1/2}-\int_{-k_p}^{k_p}dk_z\left[\left(k_z+\phi_{\omega K}+\frac{1}{2}\phi_\rho\right)^2+m_*^2\right]^{1/2}\right)\\ &+bmc_\sigma^2\left(m-m_*\right)^2+cc_\sigma^2\left(m-m_*\right)^3\ .\end{aligned} \tag{2.38}$$

The z components of neutron and proton number current densities take the form using

Eq. (2.27)

$$
\begin{aligned}
n^z &= \frac{1}{2\pi^2}\int_{-k_n}^{k_n} dk_z \left(k_z+\phi_\omega-\frac{1}{2}\phi_\rho\right)\left(\left[k_n^2+m_*^2+\phi_\omega^2-\frac{1}{4}\phi_\rho^2+2\phi_\omega k_z-\phi_\rho k_z\right]^{1/2}\right.\\
&\quad \left. -\left[\left(k_z+\phi_\omega-\frac{1}{2}\phi_\rho\right)^2+m_*^2\right]^{1/2}\right)\ ,\\
p^z &= \frac{1}{2\pi^2}\int_{-k_p}^{k_p} dk_z \left(k_z+\phi_{\omega K}+\frac{1}{2}\phi_\rho\right)\left(\left[k_p^2+m_*^2+\left(\phi_{\omega K}+\frac{1}{2}\phi_\rho\right)^2+2\left(\phi_{\omega K}+\frac{1}{2}\phi_\rho\right)k_z\right]^{1/2}\right.\\
&\quad \left. -\left[\left(k_z+\phi_{\omega K}+\frac{1}{2}\phi_\rho\right)^2+m_*^2\right]^{1/2}\right)\ . \qquad (2.39)
\end{aligned}
$$

Now we will calculate all these field coefficients, master function and pressure in the static limit $K \to 0$ to solve the background configuration of neutron star in two fluid model in next chapter 3.

2.3 Equilibrium Configuration

In this section we describe briefly the equilibrium configurations of general relativistic neutron stars in the two fluid model. To describe the spherically symmetric and static equilibrium configuration we use the metric in the Schwarzschild form

$$
\mathrm{d}s^2 = -e^{\nu(r)}\mathrm{d}t^2 + e^{\lambda(r)}\mathrm{d}r^2 + r^2\left(\mathrm{d}\theta^2+\sin^2\theta\mathrm{d}\phi^2\right)\ . \qquad (2.40)
$$

Comer et al. [53] derived the differential equations that determine the radial profiles of

$n(r)$ and $p(r)$. The equations are given by

$$\mathcal{A}_0^0\big|_0 p' + \mathcal{B}_0^0\big|_0 n' + \frac{1}{2}(B|_0 n + A|_0 p)\nu' = 0 \quad , \quad \mathcal{C}_0^0\big|_0 p' + \mathcal{A}_0^0\big|_0 n' + \frac{1}{2}(A|_0 n + C|_0 p)\nu' = 0 \tag{2.41}$$

where the time-time components are written as

$$\begin{aligned}
\mathcal{A}_0^0 &= \mathcal{A} + 2\frac{\partial \mathcal{B}}{\partial p^2} np + 2\frac{\partial \mathcal{A}}{\partial n^2} n^2 + 2\frac{\partial \mathcal{A}}{\partial p^2} p^2 + \frac{\partial \mathcal{A}}{\partial x^2} pn \,, \\
\mathcal{B}_0^0 &= \mathcal{B} + 2\frac{\partial \mathcal{B}}{\partial n^2} n^2 + 4\frac{\partial \mathcal{A}}{\partial n^2} np + \frac{\partial \mathcal{A}}{\partial x^2} p^2, \\
\mathcal{C}_0^0 &= \mathcal{C} + 2\frac{\partial \mathcal{C}}{\partial p^2} p^2 + 4\frac{\partial \mathcal{A}}{\partial p^2} np + \frac{\partial A}{\partial x^2} n^2 \,.
\end{aligned} \tag{2.42}$$

The two metric functions $\nu(r)$ and $\lambda(r)$ can be determined by solving two independent Einstein equations, which are written as

$$\lambda' = \frac{1 - e^{\lambda}}{r} - 8\pi r e^{\lambda} \left.\Lambda\right|_0 (n,p) \quad , \quad \nu' = -\frac{1 - e^{\lambda}}{r} + 8\pi r e^{\lambda} \left.\Psi\right|_0 (n,p) \,. \tag{2.43}$$

Here the symbol $|_0$ means that after the partial derivatives are taken then set $x^2 = np$. The functions $\nu(r)$, $\lambda(r)$, $n(r)$, and $p(r)$ can be determined by solving these above equations (2.41) and (2.43) to solve the background of neutron stars in the two fluid model.

A boundary condition is applied to the star surface as well as at the center of the star. A smooth joining of the interior spacetime to a Schwarzschild vacuum exterior at the surface of the star implies that the total mass M of the system is given by

$$M = -4\pi \int_0^R \mathrm{d}r\, r^2 \;\left.\Lambda\right|_0 (r), \tag{2.44}$$

and the total pressure must vanish at the surface of the star i.e $\Psi(R) = 0$. When we solve this equation using the master function, these two conditions guarantee that Ψ and Λ vanish at the surface. The regularity condition at the center of the star demands that λ, λ', ν', n_0' and p_0' vanish at the origin.

2.4 Calculation of Entrainment Parameter

The entrainment between protons and neutrons is a key component of models of neutron star superfluidity. In the section 2.1, from equations (2.2) and (2.3) we see that each fluid momentum μ^μ or χ^μ is given by a linear combination of the individual currents n^μ and p^μ. It implies that the current and momentum for a particular fluid do not have to be parallel. Two fluids in a mixture are not decoupled when one fluid interpenetrates through the other. In this situation, the momentum of one fluid is proportional to the linear combination of velocities of both fluids. This effect is known as the entrainment. This effect was found in a mixture of superfluid ^{3}He and ^{4}He in the laboratory [34]. The entrainment only vanishes in the special case where master function is independent of x^2.

The entrainment parameter was calculated in great detail in papers [36, 39, 54] based on the Newtonian calculations [55] and effective mass calculations [56]. The current and momentum for a particular fluid do not have to be parallel in the superfluid motion. To define entrainment coefficient we have to specify what we mean by the rest-frame of neutrons [39]. We have defined it by setting neutron number density current equal to zero. For this choice of frame we see from Eq. (2.2) that the momentum covector of neutrons is non zero. This choice of frame is called the zero velocity frame. Another choice of the neutron rest-frame would be possible by setting neutron momentum covector equals to zero. For this choice, the neutron number density current is non zero. This choice of the frame is called neutron zero momentum frame.

To determine the entrainment parameter, we write the relativistic analog of the mass density matrix as described by Comer and Joynt [52]

$$mn^{\mu} = \frac{\rho_{nn}}{m}\mu^{\mu} + \frac{\rho_{np}}{m}\chi^{\mu}, \tag{2.45}$$

$$mp^{\mu} = \frac{\rho_{np}}{m}\mu^{\mu} + \frac{\rho_{pp}}{m}\chi^{\mu}, \tag{2.46}$$

where ρ_{nn}, ρ_{pp} and ρ_{np} are the elements of the mass density matrix. In the non-relativistic limit this definitions reduce to Newtonian definitions. Inverting equations (2.2) and (2.3) we get

$$mn^{\mu} = \frac{m\,\mathcal{C}|_0}{\mathcal{B}|_0\,\mathcal{C}|_0 - \mathcal{A}|_0^2}\mu^{\mu} - \frac{m\,\mathcal{A}|_0}{\mathcal{B}|_0\,\mathcal{C}|_0 - \mathcal{A}|_0^2}\chi^{\mu}, \tag{2.47}$$

$$mp^{\mu} = \frac{-m\,\mathcal{A}|_0}{\mathcal{B}|_0\,\mathcal{C}|_0 - \mathcal{A}|_0^2}\mu^{\mu} + \frac{m\,\mathcal{B}|_0}{\mathcal{B}|_0\,\mathcal{C}|_0 - \mathcal{A}|_0^2}\chi^{\mu}. \tag{2.48}$$

Now the entrainment parameter (ϵ_{mom}) in the zero momentum frame of neutrons is related to the off-diagonal component of the mass density matrix i.e. $\rho_{np} = -\epsilon_{mom} mn$ [34,57]. Now comparing equations (2.47) and (2.48) with equations (2.45) and (2.46), we can calculate the entrainment parameter in terms of the background field coefficients that is given by the following relation

$$\epsilon_{mom} = \frac{m}{n}\frac{\mathcal{A}|_0}{(\mathcal{B}|_0\mathcal{C}|_0 - \mathcal{A}|_0^2)}\;. \tag{2.49}$$

In the zero velocity frame of neutrons the entrainment parameter is given by the following relation [39, 52],

$$\epsilon_{vel} = \frac{\mathcal{A}|_0 n}{m} \; . \tag{2.50}$$

CHAPTER 3

ISOSPIN DEPENDENT ENTRAINMENT IN NEUTRON STARS

3.1 Introduction

Superfluidity in neutron stars was studied in great detail in Newtonian as well as general relativistic formulations [39, 48, 58]. The fluid formalism in the case of superfluidity is different from that of the perfect fluid. For neutron stars made of neutrons, protons and electrons, two fluid formalism was used to describe the superfluidity in neutron star matter [48]. In this case, one fluid is the superfluid neutrons and the other fluid called the proton fluid represents the charge neutral component made of protons and electrons. It is a well known fact that two fluids in a mixture are not decoupled when one fluid interpenetrates through the other. In this situation, the momentum of one fluid is proportional to the linear combination of the velocities of both fluids. This effect is known as entrainment. The entrainment effect has been studied intensively in understanding rotational equilibria, oscillations of superfluid neutron stars [36–39] and the pulsar glitch [30, 31].

Superfluid dynamics including entrainment in neutron stars were studied using Newtonian calculations. The entrainment effect in nonrelativistic and relativistic Fermi-liquid models was studied by different groups [55,57,59,60]. A Similar model was developed for entrainment to study slowly rotating superfluid Newtonian neutron stars [39]. Comer and Joynt calculated the entrainment effect in a relativistic field theoretical model and obtained first order corrections to the slowly rotating superfluid neutron stars [52] for the first time. However, the relativistic model was inadequate to describe the neutron star matter because the σ-ω Walecka model was adopted in this calculation. Neutron star matter is highly asymmetric and the inclusion of ρ mesons in the Walecka model is absolutely necessary. Consequently, it is worth studying the effects of symmetry energy on the master function and superfluid dynamics in neutron stars. This motivates us to extend the calculation of Comer and Joynt [52, 61] to include ρ mesons along with scalar self-interactions.

We organise this chapter in the following way. We describe the relativistic σ-ω-ρ model for entrainment and the connection between the master function and relativistic mean field model as well as the formalism for slowly rotating superfluid neutron stars in Sec. 3.2. Results of this calculation are discussed in Sec. 3.3. Section 3.4 gives the summary and conclusions.

3.2 Formalism

Here we adopt the two fluid formalism as described in Sec. 2.1 to study the entrainment effect in cold neutron stars. The signature of the metric used here is the same as in Refs. [51, 52]. The field equations for neutrons and protons involve two conservation and two Euler equations. The master function is determined from averaged stress-energy components in a covariant way from the following relation [52, 61]

$$\Lambda = -\frac{1}{2}\langle T\rangle + \frac{3}{2}\left(x^4 - n^2p^2\right)^{-1}\left(n^2p^2\left[\frac{1}{n^2}n^\mu n^\nu + \frac{1}{p^2}p^\mu p^\nu\right] - x^2\left[n^\mu p^\nu + p^\mu n^\nu\right]\right)\langle T_{\mu\nu}\rangle \ , \tag{3.1}$$

where $\langle T\rangle = \langle T^\mu_\mu\rangle$ and the generalized pressure is

$$\Psi = \frac{1}{3}\left(\langle T\rangle - \Lambda\right) \ . \tag{3.2}$$

Similarly, one obtains the coefficients [52]

$$\mathcal{A} = \frac{-\left(n_\mu p^\nu \langle T^\mu_\nu\rangle + x^2\Lambda\right)}{\left(x^4 - n^2p^2\right)} \ , \tag{3.3}$$

$$\mathcal{B} = \frac{\left(p_\mu p^\nu \langle T^\mu_\nu\rangle + p^2\Lambda\right)}{\left(x^4 - n^2p^2\right)} \ , \tag{3.4}$$

$$\mathcal{C} = \frac{\left(n_\mu n^\nu \langle T^\mu_\nu\rangle + n^2\Lambda\right)}{\left(x^4 - n^2p^2\right)} \ . \tag{3.5}$$

Relating neutron (n^μ) and proton (p^μ) number density currents to mean particle fluxes of neutrons and protons along the z direction in the relativistic mean field (RMF) model [52], it follows from Eq.(3.1) that

$$\Lambda = \langle T^0_0\rangle + \langle T^z_z\rangle - \langle T^x_x\rangle \ , \tag{3.6}$$

where averaged stress-energy components are calculated in the RMF model and those are defined below.

Next the implications of slow rotation are discussed in the following paragraph [52].

Here it is assumed that the space-time is flat in local regions of fluid elements. Since $x^2 - np$ is small with respect to np [52], this leads to the analytic expansion of the master function as

$$\Lambda(n^2, p^2, x^2) = \sum_{i=0}^{\infty} \lambda_i(n^2, p^2) \left(x^2 - np\right)^i \ . \tag{3.7}$$

Coefficients in the field equations are given by [52],

$$\begin{aligned}
\mathcal{A} &= -\sum_{i=1}^{\infty} i \ \lambda_i(n^2, p^2) \left(x^2 - np\right)^{i-1} \ , \\
\mathcal{B} &= -\frac{1}{n}\frac{\partial \lambda_0}{\partial n} - \frac{p}{n}\mathcal{A} - \frac{1}{n}\sum_{i=1}^{\infty} \frac{\partial \lambda_i}{\partial n} \left(x^2 - np\right)^i \ , \\
\mathcal{C} &= -\frac{1}{p}\frac{\partial \lambda_0}{\partial p} - \frac{n}{p}\mathcal{A} - \frac{1}{p}\sum_{i=1}^{\infty} \frac{\partial \lambda_i}{\partial p} \left(x^2 - np\right)^i \ .
\end{aligned} \tag{3.8}$$

The master function is calculated within a RMF model [4, 52]. The detail calculations of the RMF model are discussed in Sec. 2.2. In this case, the relative motion between neutrons and protons is taken into account. In the RMF model, nucleon-nucleon interaction is mediated by the exchange of mesons. Comer and Joynt [52, 61] made the connection between the macroscopic fluid system and microscopic RMF model for the first time. They used the relativistic σ-ω model in their calculation [52]. However, neutron star matter is highly isospin asymmetric matter. This can be taken care of by the inclusion of ρ mesons in the RMF model. We extend the calculation of Comer and Joynt [52] to include ρ mesons as well as scalar meson self-interactions.

We choose a frame in which neutrons have zero spatial momentum and protons have a wave vector $k_\mu = (k_0, 0, 0, K)$ [52]. We obtain the meson field equations using equations

(2.16) and (2.19)-(2.18) of Sec. 2.2,

$$m_* = m - c_\sigma^2 \left\langle \bar{\psi}\psi \right\rangle + bmc_\sigma^2 \left(m - m_*\right)^2 + cc_\sigma^2 \left(m - m_*\right)^3 \tag{3.9}$$

$$g_\omega \omega_0 = -c_\omega^2 (n^0 + p^0) \; , \tag{3.10}$$

$$g_\omega \omega^z = -c_\omega^2 (n^z + p^z) \; , \tag{3.11}$$

$$g_\rho \rho_3^0 = -\frac{1}{2} {c_\rho}^2 (p^0 - n^0) \; , \tag{3.12}$$

$$g_\rho \rho_3^z = -\frac{1}{2} {c_\rho}^2 (p^z - n^z) \; , \tag{3.13}$$

where $p^0 = \left\langle \bar{\psi}_p \gamma^0 \psi_p \right\rangle = k_p^3 / 3\pi^2$, $n^0 = \left\langle \bar{\psi}_n \gamma^0 \psi_n \right\rangle = k_n^3 / 3\pi^2$, $p^z = \left\langle \bar{\psi}_p \gamma^z \psi_p \right\rangle$, and $n^z = \left\langle \bar{\psi}_n \gamma^z \psi_n \right\rangle$. The values of the z components of neutron and proton number current densities and the effective masses are determined by the equations (2.39) and (2.38) of Sec. 2.2. To determine the master function from Eq. (3.6) we need the values of averaged stress-energy tensor components. In the zero momentum frame of neutrons, averaged stress-energy tensor components are given by equations (2.32) -(2.35) . The master function in Eq. (3.1) can be written as [61]

$$\begin{aligned} \Lambda \;\; = \;\; & -\frac{c_\omega^2}{18\pi^4} \left(k_n^3 + k_p^3\right)^2 - \frac{c_\rho^2}{72\pi^4} \left(k_p^3 - k_n^3\right)^2 - \frac{1}{2c_\omega^2} \phi_\omega^2 - \frac{1}{2c_\rho^2} \phi_\rho^2 \\ & -\frac{1}{2c_\sigma^2} (m^2 - m_*^2) - \frac{1}{3} bm \left(m - m_*\right)^3 - \frac{1}{4} c \left(m - m_*\right)^4 \\ & -3 \sum_{B=n,p} \left\langle \bar{\psi_B} \gamma^x k_x \psi_B \right\rangle \; , \end{aligned} \tag{3.14}$$

where,

$$\sum_{B=n,p}\langle\bar{\psi}_B\gamma^x k_x\psi_B\rangle = \frac{1}{12\pi^2}\left(\int_{-k_n}^{k_n}dk_z\left[(k_n^2-2m_*^2-2\phi_\omega^2-\frac{1}{2}\phi_\rho^2-3k_z^2-4\phi_\omega k_z+2\phi_\rho k_z\right.\right.$$
$$+2\phi_\omega\phi_\rho)(k_n^2+\phi_\omega^2+\frac{1}{4}\phi_\rho^2+m_*^2+2\phi_\omega k_z-\phi_\rho k_z-\phi_\omega\phi_\rho)^{1/2}$$
$$\left.+2([k_z+\phi_\omega-\frac{1}{2}\phi_\rho]^2+m_*^2)^{3/2}\right]$$
$$+\int_{-k_p}^{k_p}dk_z\left[(k_p^2-2m_*^2-2\phi_{\omega K}^2-\frac{1}{2}\phi_\rho^2-3k_z^2-4\phi_{\omega K}k_z-2\phi_\rho k_z\right.$$
$$-2\phi_{\omega K}\phi_\rho)(k_p^2+\phi_{\omega K}^2+\frac{1}{4}\phi_\rho^2+m_*^2+2\phi_{\omega K}k_z+\phi_\rho k_z+\phi_{\omega K}\phi_\rho)^{1/2}$$
$$\left.\left.+2([k_z+\phi_{\omega K}+\frac{1}{2}\phi_\rho]^2+m_*^2)^{3/2}\right]\right). \tag{3.15}$$

In evaluating the master function as well as the coefficients, the slow rotation approximation which implies that K should be small compared with $k_{n,p}$. We are dealing with superfluidity in neutron star matter which is made of neutrons, protons and electrons. When we neglect the relative motion between neutron and proton fluids, $-\Lambda|_0$ becomes the energy density of the neutron star matter. We add the contribution of electrons to the master function (Λ). Here, electrons are treated as noninteracting relativistic particles. In the slow rotation approximation, we expand scalar and vector quantities in terms of K. Scalar quantities like m_* and Λ depend on even powers of K whereas vector quantities depend on odd powers of K. We keep terms up to K^2 in our calculation. Effective mass, z components of ω and ρ fields are expanded in the following way [52],

$$
\begin{aligned}
\phi_\omega &= \left.\frac{\partial \phi_\omega}{\partial K}\right|_0 K \ , \\
\phi_\rho &= \left.\frac{\partial \phi_\rho}{\partial K}\right|_0 K \ , \\
m_* &= m_*|_0 + \left.\frac{\partial m_*}{\partial K^2}\right|_0 K^2 \ .
\end{aligned}
\tag{3.16}
$$

Here,

$$
\begin{aligned}
m_*|_0 &= m_*(k_n, k_p, 0) \\
&= m - m_*|_0 \frac{c_\sigma^2}{2\pi^2}\Bigg(k_n\sqrt{k_n^2 + m_*^2|_0} + k_p\sqrt{k_p^2 + m_*^2|_0} \\
&\quad + \frac{1}{2}\ m_*^2\big|_0 \ln\left[\frac{-k_n + \sqrt{k_n^2 + m_*^2|_0}}{k_n + \sqrt{k_n^2 + m_*^2|_0}}\right] + \frac{1}{2}\ m_*^2\big|_0 \ln\left[\frac{-k_p + \sqrt{k_p^2 + m_*^2|_0}}{k_p + \sqrt{k_p^2 + m_*^2|_0}}\right]\Bigg) \\
&\quad + bmc_\sigma^2\left(m - m_*\right)^2 + cc_\sigma^2\left(m - m_*\right)^3 \ .
\end{aligned}
\tag{3.17}
$$

Plugging Eqs.(3.16) in Eq.(2.38) and Eq.(2.39) and expanding and keeping terms up to orders K^2, we obtain

$$\left.\frac{\partial m_*}{\partial k_n}\right|_0 = -\frac{c_\sigma^2}{\pi^2}\frac{m_*|_0\, k_n^2}{\sqrt{k_n^2+m_*^2|_0}}\left(\frac{3m-2\,m_*|_0+3bmc_\sigma^2\,(m-m_*|_0)^2+3cc_\sigma^2\,(m-m_*|_0)^3}{m_*|_0}\right.$$
$$-\frac{c_\sigma^2}{\pi^2}\left[\frac{k_n^3}{\sqrt{k_n^2+m_*^2|_0}}+\frac{k_p^3}{\sqrt{k_p^2+m_*^2|_0}}\right]$$
$$\left.+2bmc_\sigma^2\,(m-m_*|_0)+3cc_\sigma^2\,(m-m_*|_0)^2\right)^{-1}\ , \tag{3.18}$$

$$\left.\frac{\partial m_*}{\partial k_p}\right|_0 = -\frac{c_\sigma^2}{\pi^2}\frac{m_*|_0\, k_p^2}{\sqrt{k_p^2+m_*^2|_0}}\left(\frac{3m-2\,m_*|_0+3bmc_\sigma^2\,(m-m_*|_0)^2+3cc_\sigma^2\,(m-m_*|_0)^3}{m_*|_0}\right.$$
$$-\frac{c_\sigma^2}{\pi^2}\left[\frac{k_n^3}{\sqrt{k_n^2+m_*^2|_0}}+\frac{k_p^3}{\sqrt{k_p^2+m_*^2|_0}}\right]$$
$$\left.+2bmc_\sigma^2\,(m-m_*|_0)+3cc_\sigma^2\,(m-m_*|_0)^2\right)^{-1}, \tag{3.19}$$

$$n^z = \frac{1}{3\pi^2}\frac{k_n^3}{\sqrt{k_n^2+m_*^2|_0}}\left(\left.\frac{\partial\phi_\omega}{\partial K}\right|_0 K-\frac{1}{2}\left.\frac{\partial\phi_\rho}{\partial K}\right|_0 K\right), \tag{3.20}$$

$$p^z = \frac{1}{3\pi^2}\frac{k_p^3}{\sqrt{k_p^2+m_*^2|_0}}\left(\left.\frac{\partial\phi_\omega}{\partial K}\right|_0 K+\frac{1}{2}\left.\frac{\partial\phi_\rho}{\partial K}\right|_0 K+K\right)\ . \tag{3.21}$$

and also

$$p^z+n^z=-\frac{1}{c_\omega^2}\left.\frac{\partial\phi_\omega}{\partial K}\right|_0 K \tag{3.22}$$

$$p^z-n^z=-\frac{2}{c_\rho^2}\left.\frac{\partial\phi_\rho}{\partial K}\right|_0 K \tag{3.23}$$

Using the four equations above, we get

$$\left.\frac{\partial\phi_\omega}{\partial K}\right|_0 = \frac{-\frac{c_\omega^2}{3\pi^2}\frac{k_p^3}{\sqrt{k_p^2+m_*^2|_0}}\left(1+\frac{1}{4}\frac{c_\rho^2}{3\pi^2}\frac{2k_n^3}{\sqrt{k_n^2+m_*^2|_0}}\right)}{\left(1+\frac{c_\omega^2+\frac{c_\rho^2}{4}}{3\pi^2}\left[\frac{k_n^3}{\sqrt{k_n^2+m_*^2|_0}}+\frac{k_p^3}{\sqrt{k_p^2+m_*^2|_0}}\right]+\frac{c_\omega^2 c_\rho^2}{9\pi^4}\left[\frac{k_n^3 k_p^3}{\sqrt{(k_n^2+m_*^2|_0)(k_p^2+m_*^2|_0)}}\right]\right)}, \tag{3.24}$$

$$\frac{1}{2}\left.\frac{\partial\phi_\rho}{\partial K}\right|_0 = \frac{-\frac{1}{4}\frac{c_\rho^2}{3\pi^2}\frac{k_p^3}{\sqrt{k_p^2+m_*^2|_0}}\left(1+\frac{c_\omega^2}{3\pi^2}\frac{2k_n^3}{\sqrt{k_n^2+m_*^2|_0}}\right)}{\left(1+\frac{c_\omega^2+\frac{c_\rho^2}{4}}{3\pi^2}\left[\frac{k_n^3}{\sqrt{k_n^2+m_*^2|_0}}+\frac{k_p^3}{\sqrt{k_p^2+m_*^2|_0}}\right]+\frac{c_\omega^2 c_\rho^2}{9\pi^4}\left[\frac{k_n^3 k_p^3}{\sqrt{(k_n^2+m_*^2|_0)(k_p^2+m_*^2|_0)}}\right]\right)}. \tag{3.25}$$

Further we find $\frac{\partial m_*}{\partial K^2}\big|_0 = 0$.

Therefore, in the limit $K \to 0$, the master function which is the first term of Eq. (3.7), generalized pressure and the chemical potentials of neutron and proton fluids are given by

$$\begin{aligned}
\Lambda|_0 &= -\frac{c_\omega^2}{18\pi^4}\left(k_n^3+k_p^3\right)^2-\frac{c_\rho^2}{72\pi^4}\left(k_p^3-k_n^3\right)^2-\frac{1}{4\pi^2}\left(k_n^3\sqrt{k_n^2+m_*^2|_0}\right.\\
&\left.+k_p^3\sqrt{k_p^2+m_*^2|_0}\right)-\frac{1}{4}c_\sigma^{-2}\left[\left(2m-m_*|_0\right)\left(m-m_*|_0\right)\right.\\
&\left.+\,m_*|_0\left(bmc_\sigma^2\left(m-m_*|_0\right)^2+cc_\sigma^2\left(m-m_*|_0\right)^3\right)\right]\\
&-\frac{1}{3}bm\left(m-m_*|_0\right)^3-\frac{1}{4}c\left(m-m_*|_0\right)^4-\frac{1}{8\pi^2}\left(k_p\left[2k_p^2+m_e^2\right]\sqrt{k_p^2+m_e^2}\right.\\
&\left.-m_e^4\ln\left[\frac{k_p+\sqrt{k_p^2+m_e^2}}{m_e}\right]\right),
\end{aligned}\tag{3.26}$$

$$\begin{aligned}
\mu|_0 &= -\frac{\pi^2}{k_n^2}\left.\frac{\partial\Lambda}{\partial k_n}\right|_0\\
&= \frac{c_\omega^2}{3\pi^2}\left(k_n^3+k_p^3\right)-\frac{c_\rho^2}{12\pi^2}\left(k_p^3-k_n^3\right)+\sqrt{k_n^2+m_*^2|_0}\,,
\end{aligned}\tag{3.27}$$

$$\chi|_0 = -\frac{\pi^2}{k_p^2}\left.\frac{\partial\Lambda}{\partial k_p}\right|_0$$

$$= \frac{c_\omega^2}{3\pi^2}\left(k_n^3+k_p^3\right)+\frac{c_\rho^2}{12\pi^2}\left(k_p^3-k_n^3\right)+\sqrt{k_p^2+m_*^2|_0}+\sqrt{k_p^2+m_e^2}\,, \tag{3.28}$$

$$\Psi|_0 = \Lambda|_0+\frac{1}{3\pi^2}\left(\mu|_0\,k_n^3+\chi|_0\,k_p^3\right)\,, \tag{3.29}$$

where the subscript "0" stands for quantities calculated in the limit $K\to 0$. It is to be noted here that energy density $-\Lambda|_0$ and pressure $\Psi|_0$ constitute the equation of state for the calculation of equilibrium configurations of neutron stars which we discuss in Sec. 3.3.

Coefficients in momentum covectors are given by,

$$\begin{aligned}
\mathcal{A}|_0 &= c_\omega^2-\frac{1}{4}c_\rho^2+\frac{c_\omega^2}{5\,\mu^2|_0}\left(2k_p^2\frac{\sqrt{k_n^2+m_*^2|_0}}{\sqrt{k_p^2+m_*^2|_0}}+\frac{c_\omega^2}{3\pi^2}\left[\frac{k_n^2k_p^3}{\sqrt{k_n^2+m_*^2|_0}}+\frac{k_p^2k_n^3}{\sqrt{k_p^2+m_*^2|_0}}\right]\right)\\
&+\frac{c_\rho^2}{20\,\mu^2|_0}\left(2k_p^2\frac{\sqrt{k_n^2+m_*^2|_0}}{\sqrt{k_p^2+m_*^2|_0}}+\frac{c_\rho^2}{12\pi^2}\left[\frac{k_n^2k_p^3}{\sqrt{k_n^2+m_*^2|_0}}+\frac{k_p^2k_n^3}{\sqrt{k_p^2+m_*^2|_0}}\right]\right)\\
&-\frac{c_\rho^2c_\omega^2}{30\,\mu^2|_0\,\pi^2}\left[\frac{k_n^2k_p^3}{\sqrt{k_n^2+m_*^2|_0}}-\frac{k_p^2k_n^3}{\sqrt{k_p^2+m_*^2|_0}}\right]+\frac{3\pi^2k_p^2}{5\,\mu^2|_0\,k_n^3}\frac{k_n^2+m_*^2|_0}{\sqrt{k_p^2+m_*^2|_0}}\,,
\end{aligned} \tag{3.30}$$

$$\begin{aligned}
\mathcal{B}|_0 &= \frac{3\pi^2\,\mu|_0}{k_n^3}-c_\omega^2\frac{k_p^3}{k_n^3}+\frac{1}{4}c_\rho^2\frac{k_p^3}{k_n^3}\\
&-\frac{c_\omega^2k_p^3}{5\,\mu^2|_0\,k_n^3}\left(2k_p^2\frac{\sqrt{k_n^2+m_*^2|_0}}{\sqrt{k_p^2+m_*^2|_0}}+\frac{c_\omega^2}{3\pi^2}\left[\frac{k_n^2k_p^3}{\sqrt{k_n^2+m_*^2|_0}}+\frac{k_p^2k_n^3}{\sqrt{k_p^2+m_*^2|_0}}\right]\right)\\
&-\frac{c_\rho^2k_p^3}{20\,\mu^2|_0\,k_n^3}\left(2k_p^2\frac{\sqrt{k_n^2+m_*^2|_0}}{\sqrt{k_p^2+m_*^2|_0}}+\frac{c_\rho^2}{12\pi^2}\left[\frac{k_n^2k_p^3}{\sqrt{k_n^2+m_*^2|_0}}+\frac{k_p^2k_n^3}{\sqrt{k_p^2+m_*^2|_0}}\right]\right)\\
&+\frac{c_\rho^2c_\omega^2k_p^3}{30\pi^2\,\mu^2|_0\,k_n^3}\left[\frac{k_n^2k_p^3}{\sqrt{k_n^2+m_*^2|_0}}-\frac{k_p^2k_n^3}{\sqrt{k_p^2+m_*^2|_0}}\right]-\frac{3\pi^2k_p^5}{5\,\mu^2|_0\,k_n^6}\frac{k_n^2+m_*^2|_0}{\sqrt{k_p^2+m_*^2|_0}}
\end{aligned} \tag{3.31}$$

$$\mathcal{C}|_0 = \frac{3\pi^2\,\chi|_0}{k_p^3}+\frac{1}{4}c_\rho^2\frac{k_n^3}{k_p^3}-c_\omega^2\frac{k_n^3}{k_p^3}$$

$$
\begin{aligned}
&-\frac{c_\omega^2 k_n^3}{5\,\mu^2|_0\,k_p^3}\left(2k_p^2\frac{\sqrt{k_n^2+m_*^2|_0}}{\sqrt{k_p^2+m_*^2|_0}}+\frac{c_\omega^2}{3\pi^2}\left[\frac{k_n^2k_p^3}{\sqrt{k_n^2+m_*^2|_0}}+\frac{k_p^2k_n^3}{\sqrt{k_p^2+m_*^2|_0}}\right]\right)\\
&-\frac{c_\rho^2 k_n^3}{20\,\mu^2|_0\,k_p^3}\left(2k_p^2\frac{\sqrt{k_n^2+m_*^2|_0}}{\sqrt{k_p^2+m_*^2|_0}}+\frac{c_\rho^2}{12\pi^2}\left[\frac{k_n^2k_p^3}{\sqrt{k_n^2+m_*^2|_0}}+\frac{k_p^2k_n^3}{\sqrt{k_p^2+m_*^2|_0}}\right]\right)\\
&+\frac{c_\rho^2 c_\omega^2 k_n^3}{30\pi^2\,\mu^2|_0\,k_p^3}\left[\frac{k_n^2k_p^3}{\sqrt{k_n^2+m_*^2|_0}}-\frac{k_p^2k_n^3}{\sqrt{k_p^2+m_*^2|_0}}\right]-\frac{3\pi^2}{5\,\mu^2|_0\,k_p}\frac{k_n^2+m_*^2|_0}{\sqrt{k_p^2+m_*^2|_0}}\,. \qquad (3.32)
\end{aligned}
$$

Similarly, other coefficients which enter into the calculation of equilibrium neutron star configurations, are calculated according to Ref. [52] and given by,

$$
\begin{aligned}
\mathcal{A}_0^0|_0 &= -\frac{\pi^4}{k_p^2k_n^2}\left.\frac{\partial^2\Lambda}{\partial k_p\partial k_n}\right|_0\\
&= c_\omega^2-\frac{c_\rho^2}{4}+\frac{\pi^2}{k_p^2}\frac{m_*|_0\left.\frac{\partial m_*}{\partial k_p}\right|_0}{\sqrt{k_n^2+m_*^2|_0}}\,, \qquad (3.33)\\
\mathcal{B}_0^0|_0 &= \frac{\pi^4}{k_n^5}\left(2\left.\frac{\partial\Lambda}{\partial k_n}\right|_0-k_n\left.\frac{\partial^2\Lambda}{\partial k_n^2}\right|_0\right)\\
&= c_\omega^2+\frac{c_\rho^2}{4}+\frac{\pi^2}{k_n^2}\frac{k_n+m_*|_0\left.\frac{\partial m_*}{\partial k_n}\right|_0}{\sqrt{k_n^2+m_*^2|_0}}\,, \qquad (3.34)\\
\mathcal{C}_0^0|_0 &= \frac{\pi^4}{k_p^5}\left(2\left.\frac{\partial\Lambda}{\partial k_p}\right|_0-k_p\left.\frac{\partial^2\Lambda}{\partial k_p^2}\right|_0\right)\\
&= c_\omega^2+\frac{c_\rho^2}{4}+\frac{\pi^2}{k_p^2}\frac{k_p+m_*|_0\left.\frac{\partial m_*}{\partial k_p}\right|_0}{\sqrt{k_p^2+m_*^2|_0}}+\frac{\pi^2}{k_p}\frac{1}{\sqrt{k_p^2+m_e^2}}\,. \qquad (3.35)
\end{aligned}
$$

Derivatives of the effective mass with respect to neutron and proton Fermi momenta are explicitly shown in equations (3.18) and (3.19) .

We obtain entrainment matrix elements inverting Eqs. (2.2) and (2.3) and compare those with the relativistic analog of the mass density matrix (ρ_{ik}) [34, 52],

$$
\begin{aligned}
Y_{nn} &= \frac{\rho_{nn}}{m^2} = \frac{\mathcal{C}|_0}{(\mathcal{B}|_0\mathcal{C}|_0 - \mathcal{A}|_0^2)} , \\
Y_{np} &= \frac{\rho_{np}}{m^2} = -\frac{\mathcal{A}|_0}{(\mathcal{B}|_0\mathcal{C}|_0 - \mathcal{A}|_0^2)} , \\
Y_{pp} &= \frac{\rho_{pp}}{m^2} = \frac{\mathcal{B}|_0}{(\mathcal{B}|_0\mathcal{C}|_0 - \mathcal{A}|_0^2)} .
\end{aligned}
\tag{3.36}
$$

The entrainment matrix in this form can be compared with that of Ref. [60]. It is worth noting here that when Eqs. (2.2) and (2.3) are inverted and neutron and proton number density currents are written in terms of chemical potentials, we obtain the relation $\sum_{k=n,p} Y_{ik}\mu_k = n_i$, where $i = n, p$.

Now the entrainment parameter (ϵ_{mom}) in the zero momentum frame of neutrons is related to the off-diagonal component of the mass density matrix i.e. $\rho_{np} = -\epsilon_{mom} mn$ and can be calculated in terms of coefficients in momentum covectors in two fluid formalism from the following relation [52],

$$
\epsilon_{mom} = \frac{m}{n} \frac{\mathcal{A}|_0}{(\mathcal{B}|_0\mathcal{C}|_0 - \mathcal{A}|_0^2)} . \tag{3.37}
$$

Similarly, the entrainment parameter in the zero velocity frame of neutrons is given by [39, 52],

$$
\epsilon_{vel} = \frac{\mathcal{A}|_0 n}{m} . \tag{3.38}
$$

In the nonrelativistic case, an explicit relationship between the entrainment parameter and effective nucleon mass was found by various groups [39, 57].

Table 3.1: Nucleon-meson coupling constants in the GL and NL3 sets are taken from Refs. [4, 62]. The coupling constants are obtained by reproducing the saturation properties of symmetric nuclear matter as detailed in the text. All the parameters are in fm^2, except b and c which are dimensionless. [40]

	c_σ^2	c_ω^2	c_ρ^2	b	c
GL	12.684	7.148	4.410	0.005610	-0.006986
NL3	15.739	10.530	5.324	0.002055	-0.002650

Finally, charge neutrality and β-equilibrium conditions are to be imposed in neutron star matter. The charge neutrality condition is $k_p = k_e$. The condition of chemical equilibrium for npe matter is $\mu|_0 = \chi|_0$, where $\mu|_0$ and $\chi|_0$ are the neutron and proton plus electron chemical potentials, respectively [53, 63].

3.3 Results and Discussion

Meson-nucleon couplings c_σ, c_ω, c_ρ, b and c of the Lagrangian density in Eq. (2.10) are determined by reproducing nuclear matter saturation properties such as binding energy per nucleon (-16.3 MeV), saturation density ($n_0 = 0.153$ fm^{-3}), Dirac nucleon effective mass ($m_*/m = 0.7$), the symmetry energy coefficient (32.5 MeV) and incompressibility (200 MeV). These coupling constants are taken from the Ref. [4]. This parameter set is known as the GL set. We also perform the calculation using the non-linear (NL3) interaction [64]. New parametrization of the NL3 interaction reproducing binding energy per nucleon (-16.24 MeV), saturation density (0.148 fm^{-3}), incompressibility (271.5 MeV), the symmetry energy coefficient (37.29 MeV) and the slope of the symmetry energy (118.2 MeV) [62], is adopted in our calculation. Both parameter sets are listed in Table 3.1. In this calculation, we consider the β-equilibrated neutron star matter made of neutrons (n), protons (p) and electrons (e). Equilibrium configurations of neutron stars are calculated following the prescription of Comer and other collaborators [52, 53] and using our equation of state as given by energy density ($-\Lambda|_0$) and pressure ($\Psi|_0$) in Eqs. (3.26) and (3.29), respectively. Neutron and proton Fermi momenta at the center of the star are needed for this purpose. For a given value of neutron Fermi momentum or wave number, proton Fermi momentum is calculated from the β-equilibrium condition. We perform this calculation for the GL and NL3 parameter sets. Neutron star masses as a function of central neutron density for NL3 (solid line) and GL (dashed line) sets are plotted in Fig. 3.1. It is noted that maximum neutron star masses corresponding to the GL and NL3 parameters are well above the observed limit of 2.01$\pm$0.04 $M_\odot$ [1].

For the calculation of entrainment, we choose neutron star configurations which are just

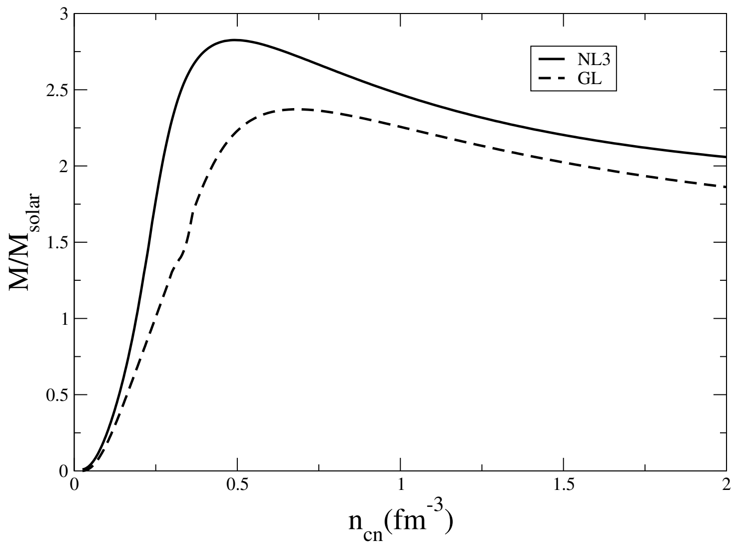

Figure 3.1: Neutron star sequence is plotted with central neutron density. The dashed line corresponds to the calculation with the GL parameter set whereas the solid line implies that of the NL3 parameter set [40].

below maximum masses in both cases. In the case of the GL set, we consider a neutron star mass of 2.37 $M_{\odot}$ corresponding to the central value of neutron wave number $k_n(0) = 2.71 fm^{-1}$ and proton fraction 0.24. The radius of the neutron star is 11.09 km. Similarly, in the other case with the NL3 set, we find a neutron star having maximum mass 2.82 $M_{\odot}$ and radius 13.17 km. The corresponding central values of neutron wave number and proton fraction are 2.40 fm^{-1} and 0.23, respectively.

We calculate dynamical neutron and proton effective masses [58] using $\bar{m}_*^n = n_n \mathcal{B}|_0$

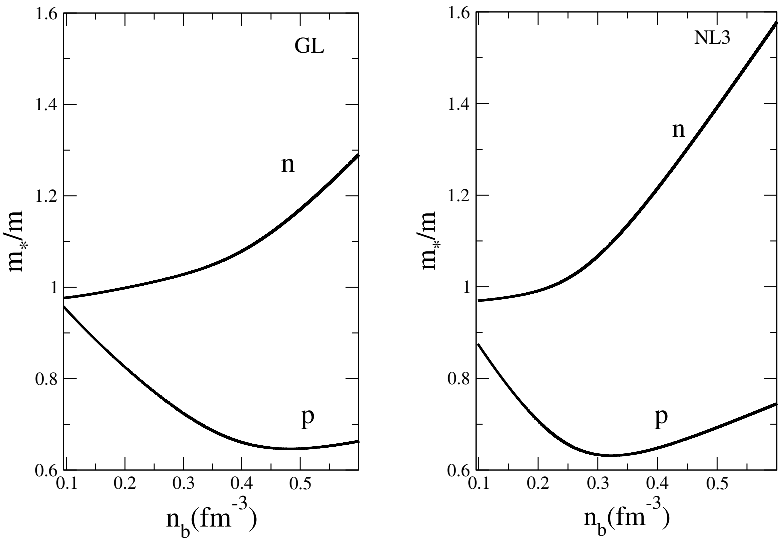

Figure 3.2: Dynamical neutron and proton effective masses are shown as a function of baryon density for the GL (left panel) and NL3 (right panel) parameter sets [40].

and $\bar{m}_*^p = n_p \mathcal{C}|_0$, where n_n and n_p are neutron and proton number densities. Dynamical effective masses are plotted as a function of baryon density in Fig. 3.2. The left panel shows the results of the GL parameter set whereas the right panel denotes those of the NL3 parameter set. In both panels, the upper curve represents the neutron effective mass and the lower curve corresponds to the proton effective mass. It is noted that the neutron effective mass increases with density and becomes greater than the free neutron mass in both cases. However, it rises faster in the NL3 case. On the other hand, the proton effective mass decreases with density initially and rises at higher densities. However, its value always stays below the free proton mass. In the GL case, the proton effective mass is always higher than that of the NL3 case. These findings are different from the effective masses calculated in the nonrelativistic calculations as noted already in Refs. [57, 58].

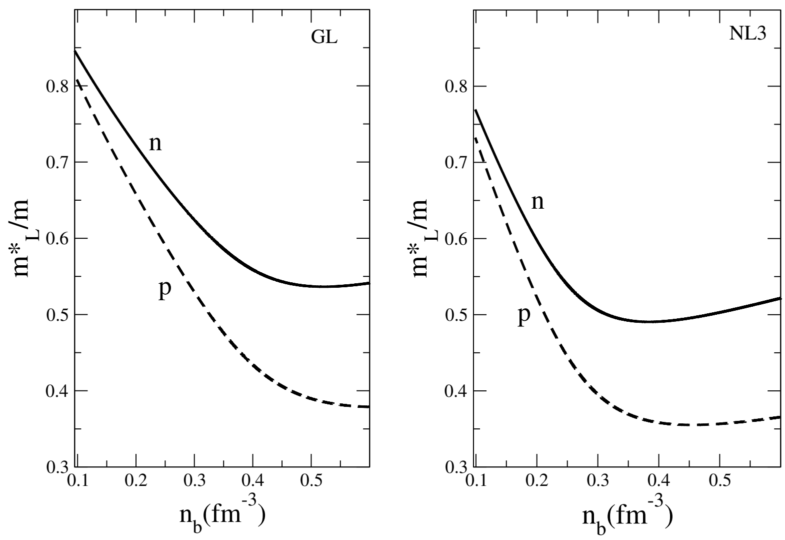

Figure 3.3: Landau effective masses are shown as a function of baryon density for the GL (left panel) and NL3 (right panel) parameter sets [40].

We also calculate the Landau effective mass for nucleons and it is related to the Dirac effective mass through the expression $m_L^{*i} = \sqrt{{k_i}^2 + (m - g_\sigma \sigma)^2}$ [60]. Landau effective masses for neutrons and protons are shown as a function of baryon density in Fig. 3.3. The left panel shows the results of the GL set and the right panel represents those of the NL3 set. Here we find that neutron and proton effective masses decrease as baryon density increases in both panels and they are below their bare masses. It is noted that the Landau effective masses are always higher in the GL set than those of the NL3 set.

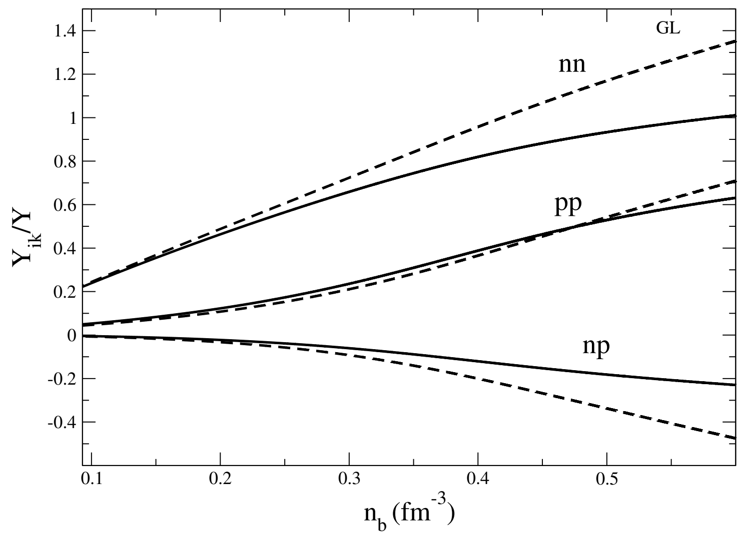

Figure 3.4: Normalised entrainment matrix elements (Y_{ik}/Y) in the zero momentum frame is plotted as a function of baryon density [40]. The normalisation factor is taken as $Y = 3n_0/\mu_n(3n_0)$ [60] where n_0 is the saturation density. Results of this calculation (dashed line) are compared with those (solid line) of Ref. [60].

Normalized entrainment matrix elements of Eq.(3.36) are shown as a function of baryon density in Fig. 3.4. The normalisation constant is chosen as $Y = 3n_0/\mu_n(3n_0)$ as it was done in Ref. [60]. Entrainment matrix elements obtained in this calculation are compared with those calculated in the relativistic Landau Fermi liquid theory [60]. Both calculations are performed using the GL set of Table I. Solid lines represent the results of Ref. [60]

whereas dashed lines demonstrate the results of Eq. (3.36) using the GL set. Though the results of the two calculations are qualitatively similar, those are quantitatively very different. The difference between the results of the two calculations is negligible initially because the entrainment effect becomes small in the low density region in both approaches. On the other hand, this difference grows at higher baryon densities as the entrainment effect becomes more dominant in our case than that of Ref. [60]. This may be attributed to different formalisms in two calculations . We also compare normalised matrix elements calculated in our model using the GL and NL3 parameter sets in Fig. 3.5. Results of the NL3 set are higher than those of the GL set. The difference in the equations of state for the two parameter sets is reflected in the results of matrix element calculations.

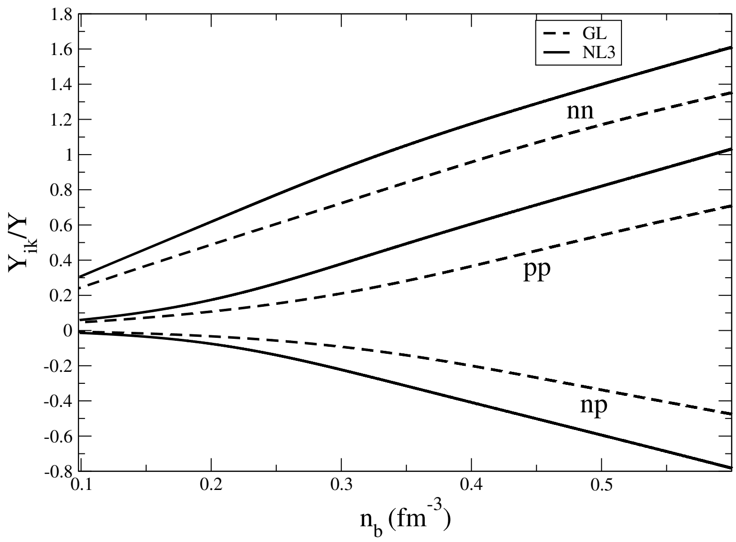

Figure 3.5: Normalised entrainment matrix elements (Y_{ik}/Y) in the zero momentum frame is plotted as a function of baryon density for the GL and NL3 parameter sets. The normalisation factor is taken as $Y = 3n_0/\mu_n(3n_0)$ [60] where n_0 is the saturation density [40].

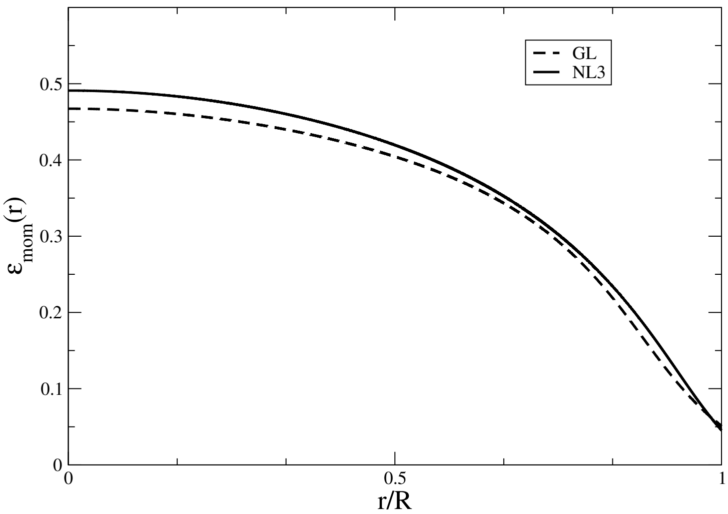

Figure 3.6: Entrainment parameter in the RMF model with ρ meson in the zero momentum frame of neutrons is plotted as a function of radial distance in a neutron star of mass $2.37M_{\odot}$ and radius 11.09 km using the GL parameter set (dashed line) and mass $2.82M_{\odot}$ and radius 13.17 km with the NL3 parameter set (solid line) [40].

Next we present the results of entrainment parameters in the zero momentum and zero velocity frames of neutrons. The radial profiles of the entrainment parameter in the zero momentum frame for the GL and NL3 sets are shown in Fig. 3.6. These radial profiles are obtained for neutron stars of mass $M = 2.37M_{\odot}$ and radius $R = 11.09$ km in the case of the GL set and $M = 2.82M_{\odot}$ and radius $R = 13.17$ km in the case of the NL3 set. The entrainment parameter in both cases remains constant in the core and drops rapidly at the surface. We find an appreciable difference between the two results towards the center. Moreover, in both cases, the entrainment effect is strong at higher baryon densities in the core whereas this effect diminishes sharply at lower densities towards the surface. The value of the entrainment parameter lies in the physical range $0 \leq \epsilon_{mom} \leq 1$ as found in earlier calculations [39, 57]. We compare this result with that of the situation excluding ρ mesons which was actually studied in Ref. [52], as displayed in Fig. 3.7 for the GL set. For

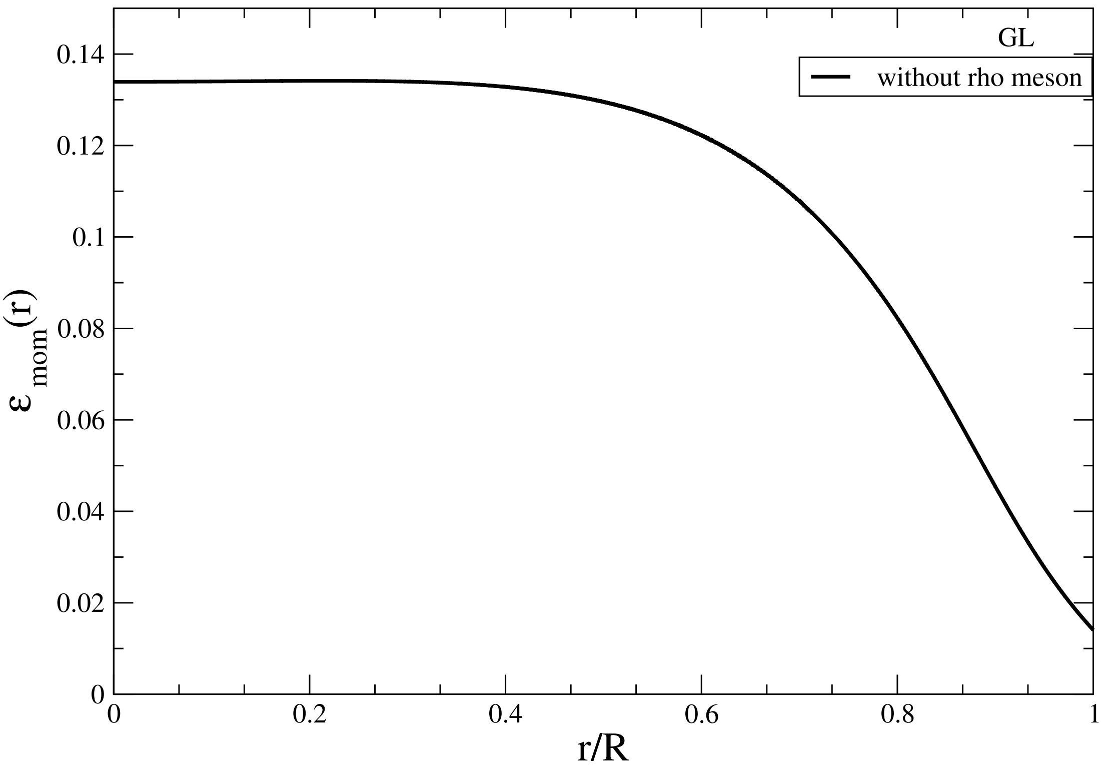

Figure 3.7: Entrainment parameter in the RMF model without ρ meson in the zero momentum frame of neutrons is plotted as a function of radial distance in a neutron star of mass 2.33 $M_{\odot}$ and radius 10.96 km. [40].

the calculation of the entrainment parameter without ρ mesons, we obtain the radial profile of the entrainment parameter in a neutron star of mass 2.33 $M_{\odot}$ and radius 10.96 km. It is evident from Figs. 3.6 and Fig. 3.7 that the inclusion of ρ in the calculation strongly enhances the entrainment parameter.

Further the radial profile of the entrainment parameter (ϵ_{vel}) in the zero velocity frame

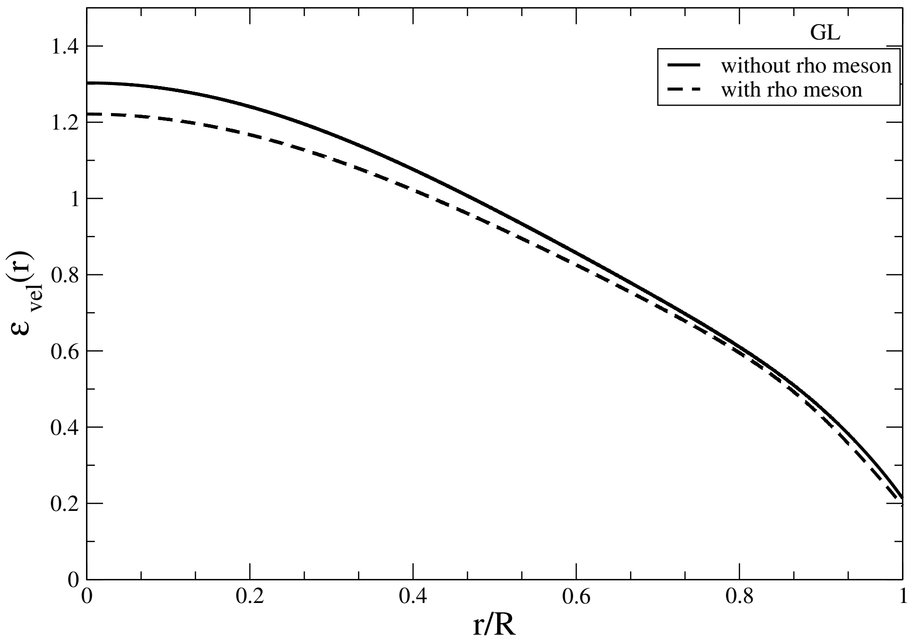

Figure 3.8: Entrainment parameter in the zero velocity frame of neutrons is plotted as a function of radial distance in neutron stars of masses 2.33 $M_\odot$ (solid line) and 2.37 $M_\odot$ (dashed line) [40].

is exhibited in Fig. 3.8. The solid line denotes the calculation without ρ mesons and the dashed line implies the case including ρ mesons. It is noted that the entrainment parameter calculated without ρ mesons is larger compared with the entrainment parameter with ρ meson. This finding is opposite to what we see in the calculation of the entrainment parameter in the zero momentum frame. We also find that the values of the entrainment parameter in the zero velocity frame are higher than those of the entrainment parameter in the zero momentum frame. Finally, we compare the radial profiles of entrainment parameters in the

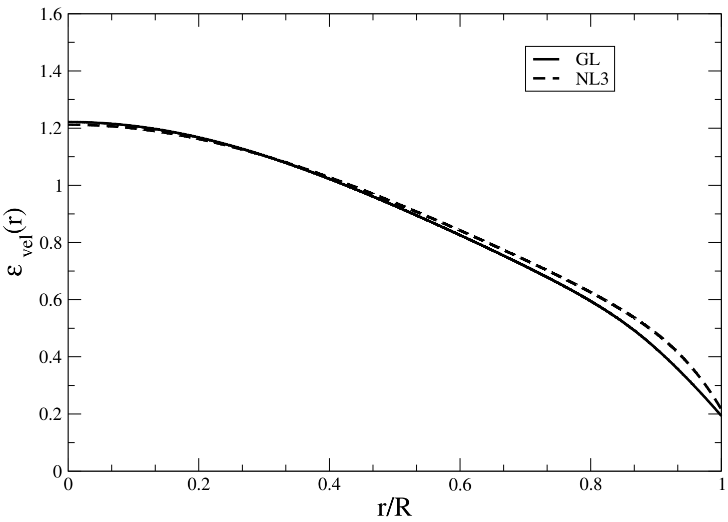

Figure 3.9: Entrainment parameter in the zero velocity frame of neutrons is plotted as a function of radial distance in neutron stars of masses 2.37 $M_\odot$ (solid line) and 2.82 $M_\odot$ (dashed line) for the GL and NL3 parameter sets, respectively [40].

zero velocity frame for the GL and NL3 parameter sets as shown in Fig. 3.9. It is evident from the figure that the two results do not differ much.

So far we have neglected muons in our calculation. However, muons can be populated in neutron star matter when the threshold condition involving electron and muon chemical potentials, $\mu_e = \mu_\mu$ is satisfied. We repeat our calculation including muons. However, muons have negligible effects on the entrainment matrix elements and entrainment parameter.

3.4 Summary and Conclusions

In this chapter we have extended the calculation of Comer and Joynt [52] to include ρ mesons and the self-interaction term in the RMF model. Here we calculate entrainment matrix elements and entrainment parameters using this model and the GL and NL3 parameter sets. It is noted that the entrainment parameter in the zero momentum frame is significantly enhanced due to the presence of ρ mesons in the calculation. Furthermore we compare our results with those of the relativistic Landau Fermi liquid theory [60] and find appreciable differences.

Our calculation may be extended to include hyperons in a straightforward manner using a three fluid description [48] and applied to study the dynamics of superfluid neutron stars. This could be compared with the findings of earlier calculations including hyperons in the relativistic Landau Fermi liquid theory [60, 65].

CHAPTER 4

SLOWLY ROTATING NEUTRON STARS WITH ENTRAINMENT

4.1 Introduction

In Chapter 3, we discussed about the entrainment effect in the the RMF model including ρ mesons [40]. We showed that the symmetry energy significantly effected the entrainment effect compared to the case without ρ mesons [40]. It may be worth mentioning here that the dependence of the entrainment effect on the symmetry energy was also studied using polytropic equations of state [39, 66] as well as with the relativistic Fermi liquid theory [55, 57, 59, 60].

The role of the entrainment effect in rotating neutron stars was investigated in Newtonian as well as general relativistic formulations by different groups [39, 61, 66]. In some of those calculations, the dependence of the entrainment effect on the symmetry energy was considered through the polytropic EoS [39, 66]. However, so far, there is no calculation of rotating neutron stars based on the isospin dependent entrainment effect derived from a realistic EoS.

This chapter is based on our paper [67]. Here we are interested to describe the role of isospin dependent entrainment on slowly rotating superfluid neutron stars. Here we adopt the two-fluid formalism for slowly rotating superfluid neutron stars as described in Sec.2.1. The chapter is organised in the following way. In Sec. 4.2 we describe the application of Hartle's slow rotation approximation to Einstein's field equations for superfluid neutron stars. We discuss results in Sec. 4.3. Section 4.4 gives the summary and conclusions.

4.2 Methodology

4.2.1 Slowly rotating superfluid neutron stars

Andersson and Comer [42] extended Hartle's slow rotation formalism for the single fluid [68] to the case of the two-fluid model in order to describe superfluid neutron stars. They considered that the superfluid neutron and the proton fluid are rotating with different rotational velocities. However, they did not include the entrainment effect in their calculation. Here we adopt the two-fluid formalism of Andersson and Comer as described by Refs. [42, 61] to study stationary, axisymmetric, and asymptotically flat configurations. Furthermore we introduce the isospin dependent entrainment in this calculation. In the slow rotation approximation, rotational velocities of neutron (Ω_n) and proton (Ω_p) fluids are considered as small so that inequalities $\Omega_n R << c$ and $\Omega_p R << c$ are satisfied, where c is the speed of light and R is the radius of the neutron star. The slow rotation acts as the perturbation on nonrotating configurations. We retain terms up to second order in the angular velocities of neutron and proton fluids in field equations in the slow rotation approximation. The metric used here has the following structure [42, 61, 68]:

$$g_{\mu\nu}\mathrm{d}x^{\mu}\mathrm{d}x^{\nu} = -(N^2-\sin^2\theta K[N^{\phi}]^2)\mathrm{d}t^2+V\mathrm{d}\tilde{r}^2-2KN^{\phi}\sin^2\theta\mathrm{d}t\mathrm{d}\phi+K\left(\mathrm{d}\theta^2+\sin^2\theta\mathrm{d}\phi^2\right) . \tag{4.1}$$

The equations relevant for the metric variables in the two-fluid model and the slow rotation approximation are same as those of Hartle's single-fluid model and the metric functions are expanded in powers of angular velocities [42, 61, 68],

$$\begin{aligned} N &= e^{\nu(\tilde{r})/2}\left(1+h(\tilde{r},\theta)\right) , \\ V &= e^{\lambda(\tilde{r})}\left(1+2v(\tilde{r},\theta)\right) , \\ K &= \tilde{r}^2(1+2k(\tilde{r},\theta)) , \\ N^{\phi} &= \omega(\tilde{r}) , \end{aligned} \tag{4.2}$$

where ω is a first order quantity in angular velocities, and h, v, and k are second order quantities. Further h, v, and k are decomposed into $\ell = 0$ and $\ell = 2$ terms after expanding those in spherical harmonics,

$$\begin{aligned} h &= h_0(\tilde{r}) + h_2(\tilde{r})P_2(\cos\theta) , \\ v &= v_0(\tilde{r}) + v_2(\tilde{r})P_2(\cos\theta) , \\ k &= k_2(\tilde{r})P_2(\cos\theta) , \end{aligned} \tag{4.3}$$

where $P_2(\cos\theta) = (3\cos^2\theta - 1)/2$.

Similarly, neutron (n) and proton (p) number densities are expanded as

$$n = n_0(\tilde{r})\,(1 + \eta(\tilde{r},\theta)) \quad , \quad p = p_0(\tilde{r})\,(1 + \Phi(\tilde{r},\theta)) \; , \tag{4.4}$$

where terms η and Φ are of $\mathcal{O}(\Omega^2_{n,p})$,

$$\eta = \eta_0(\tilde{r}) + \eta_2(\tilde{r})P_2(\cos\theta) \quad , \quad \Phi = \Phi_0(\tilde{r}) + \Phi_2(\tilde{r})P_2(\cos\theta) \; . \tag{4.5}$$

A coordinate transformation $\tilde{r} \to r + \xi(r,\theta)$ is introduced such that $\Lambda(\tilde{r}(r,\theta),\theta) = \Lambda_0(r)$ [42]. Here the ξ coordinate is also expanded in spherical harmonics as $\xi = \xi_0(r) + \xi_2(r)P_2(\cos\theta)$.

With this prescription of the slow rotation approximation for metric functions as well as neutron and proton densities along with the coordinate transformation, the fluid and Einstein field equations are reduced to four sets of equations. The first set of equations corresponds to nonrotating background configurations that are obtained from the solutions of two background metric components λ and ν [42, 61]. Those are given in terms of coefficients of fluid equations,

$$A^0_0\big|_0\, p_0' + B^0_0\big|_0\, n_0' + \frac{1}{2}\, \mu|_0\, \nu' = 0 \quad , \quad C^0_0\big|_0\, p_0' + A^0_0\big|_0\, n_0' + \frac{1}{2}\, \chi|_0\, \nu' = 0 \; , \tag{4.6}$$

where prime denotes differentiation with respect to $\tilde{r}$ and $A^0_0|_0$, $B^0_0|_0$, and $C^0_0|_0$ coefficients are obtained from the master function and are taken from chapter 3.

For the slow rotation approximation, we are interested in terms up to second order in the rotational velocities of neutrons and protons. This corresponds to the terms proportional to $x^2 - np$ in the master function. It may be noted that the following combinations appearing in the field equations are dependent on λ_1 when computed on the background [61]:

$$\mathcal{A} + n\frac{\partial \mathcal{A}}{\partial n} + np\frac{\partial \mathcal{A}}{\partial x^2} = -\lambda_1 - n\frac{\partial \lambda_1}{\partial n} - \sum_{i=2}^{\infty}\left(\lambda_i + n\frac{\partial \lambda_i}{\partial n}\right)\left(x^2 - np\right)^{i-1} , \tag{4.7}$$

$$\mathcal{A} + p\frac{\partial \mathcal{A}}{\partial p} + np\frac{\partial \mathcal{A}}{\partial x^2} = -\lambda_1 - p\frac{\partial \lambda_1}{\partial p} - \sum_{i=2}^{\infty}\left(\lambda_i + p\frac{\partial \lambda_i}{\partial p}\right)\left(x^2 - np\right)^{i-1} . \tag{4.8}$$

Here λ_1 is connected to the second term of Eq. 3.7.

Next, the frame dragging $\omega(r)$, which is first order in angular velocities of neutron and proton fluids, is obtained from the following equation [61, 68]

$$\frac{1}{r^4}\frac{d}{dr}\left(r^4 e^{-(\lambda+\nu)/2}\frac{d\tilde{L}_n}{dr}\right) - 16\pi e^{(\lambda-\nu)/2}\left(\Psi_0 - \Lambda_0\right)\tilde{L}_n = 16\pi e^{(\lambda-\nu)/2}\chi_0 p_0\left(\Omega_n - \Omega_p\right) . \tag{4.9}$$

This equation has the same structure as that of the single fluid except for the nonzero term on the right-hand side [68]. Here we define $\tilde{L}_n = \omega - \Omega_n$ and $\tilde{L}_p = \omega - \Omega_p$, which represent the rotational frequencies as measured by a distant observer. The boundary condition implies that the interior solution of $\omega(r)$ matches with the vacuum solution

$$\tilde{L}_n(R) = -\Omega_n + \frac{2J}{R^3} , \tag{4.10}$$

where J is the total angular momentum of the system. The derivative of the solution is also continuous at the surface [61].

The neutron and proton angular momenta, J_n and J_p, respectively, are given by [42]

$$J_n = -\frac{8\pi}{3}\int_0^R \mathrm{d}r r^4 e^{(\lambda-\nu)/2}\left[\mu_0 n_0 \tilde{L}_n + A_0 n_0 p_0\left(\Omega_n - \Omega_p\right)\right] \tag{4.11}$$

and

$$J_p = -\frac{8\pi}{3}\int_0^R \mathrm{d}r r^4 e^{(\lambda-\nu)/2}\left[\chi_0 p_0 \tilde{L}_p + A_0 n_0 p_0 \left(\Omega_p - \Omega_n\right)\right] . \tag{4.12}$$

The total angular momentum J is equal to $J_n + J_p$.

The last two sets of equations are $\mathcal{O}(\Omega^2_{n,p})$ equations. One can obtain ξ_0, η_0, Φ_0, h_0, and v_0 from $\ell = 0$ second-order equations, on the other hand, ξ_2, η_2, Φ_2, h_2, v_2, and k_2 follow from $\ell = 2$ second-order equations. A detailed discussion of $\ell = 0$ and $\ell = 2$ second order equations and numerical techniques to solve those equations can be found in Refs. [42, 61, 68]. After obtaining a complete solution in the slow rotation approximation, one can calculate the quadruple moment of the configuration and the rotationally induced change of mass as described in Refs. [42, 61]. We get the expression of kepler frequency upto second order of rotational velocity from equation (76) of the paper Andersson and Comer [42]

$$\Omega_k = \sqrt{\frac{e^\nu \nu'}{2\tilde{r}}} + \omega + \omega'\tilde{r}/2 + \sqrt{\frac{e^\nu \nu'}{2\tilde{r}}}(h - k + \frac{h'}{\nu'} - \tilde{r}k'/2 + \frac{\omega'^2 \tilde{r}^3}{4\nu' e^\nu}) + O(\Omega^3). \tag{4.13}$$

The vacuum solutions are

$$\omega(r) = \frac{2J}{r^3} , \tag{4.14}$$

$$h_0(r) = -\frac{\delta M}{r - 2M} + \frac{J^2}{r^3(r - 2M)} , \tag{4.15}$$

$$h_2(r) = -A\left[\frac{3}{2}\left(\frac{r}{M}\right)^2\left(1 - \frac{2M}{r}\right)\ln\left(1 - \frac{2M}{r}\right) + \frac{(r - M)\left(3 - 6M/r - 2(M/r)^2\right)}{M(1 - 2M/r)}\right] + \frac{J^2}{Mr^3}\left(1 + \frac{M}{r}\right) , \tag{4.16}$$

$$
\begin{aligned}
k_2(r) &= A\left[\frac{3}{2}\left(\frac{r}{M}\right)^2\left(1-\frac{2M^2}{r^2}\right)\ln\left(1-\frac{2M}{r}\right)+\frac{3(r-M)-8(M/r)^2\,(r-M/2)}{M(1-2M/r)}\right]- \\
&\quad \frac{J^2}{Mr^3}\left(1+\frac{2M}{r}\right)\,. \qquad (4.17)
\end{aligned}
$$

Using above four vacuum solutions we calculate the Kepler frequency upto second order of rotational velocity . The transformation $\tilde{r} \to r$ effects only the first term of Eq. (4.13). At equator $\tilde{r} \to R+\xi_0-\frac{\xi_2}{2}$, and the kepler frequency is given by

$$
\begin{aligned}
\Omega_k &= \sqrt{\frac{e^{\nu}\nu'}{2\tilde{r}}}+\omega+\omega'\tilde{r}/2+\sqrt{\frac{e^{\nu}\nu'}{2\tilde{r}}}(h-k+\frac{h'}{\nu'}-\tilde{r}k'/2+\frac{\omega'^2\tilde{r}^3}{4\nu'e^{\nu}})+O(\Omega^3) \\
&= \sqrt{\frac{M}{\tilde{r}^3}}+\frac{2J}{R^3}-\frac{\tilde{r}}{2}\frac{6J}{R^4} \\
&\quad +\sqrt{\frac{M}{\tilde{r}^3}}\left(h_0+\frac{1}{2}(k_2-h_2)+\frac{h'}{\nu'}-Rk'/2+\frac{\left(\frac{-6J}{R^4}\right)^2R^3}{4\nu'e^{\nu}}\right)+O(\Omega^3) \\
&= \sqrt{\frac{M}{(R+\xi_0-\frac{\xi_2}{2})^3}}+\frac{2J}{R^3}-\frac{3J}{R^3} \\
&\quad +\sqrt{\frac{M}{R^3}}\left(h_0+\frac{1}{2}(k_2-h_2)+\frac{h_0'}{\nu'}-\frac{h_2'}{2\nu'}+\frac{Rk_2'}{4}+\frac{18MRJ^2}{4M^2R^4}\right)+O(\Omega^3) \\
&= \sqrt{\frac{M}{R^3}}\left(1-\frac{3}{4}\frac{2\xi_0-\xi_2}{R}\right)-\frac{J}{R^3} \\
&\quad +\sqrt{\frac{M}{R^3}}\left(\frac{\delta M}{2M}+\frac{(R+3M)(3R-2M)J^2}{4M^2R^4}+\alpha A\right)+O(\Omega^3) \\
&= \sqrt{\frac{M}{R^3}}-\frac{J}{R^3}+\sqrt{\frac{M}{R^3}} \\
&\quad \left\{\frac{\delta M}{2M}+\frac{(R+3M)(3R-2M)}{4R^4M^2}J^2-\frac{3}{4}\frac{2\xi_0-\xi_2}{R}+\alpha A\right\}+O(\Omega^3). \qquad (4.18)
\end{aligned}
$$

So the final form of Kepler frequency is given by

$$\Omega_K = \sqrt{\frac{M}{R^3}} - \frac{\hat{J}\Omega_p}{R^3} + \sqrt{\frac{M}{R^3}} \left\{ \frac{\delta\hat{M}}{2M} + \frac{(R+3M)(3R-2M)}{4R^4M^2}\hat{J}^2 - \frac{3}{4}\frac{2\hat{\xi}_0 - \hat{\xi}_2}{R} + \alpha\hat{A} \right\} \Omega_p^2 , \tag{4.19}$$

where scaling of $J = \hat{J}\Omega_p$, $\delta M = \delta\hat{M}\Omega_p^2$, $\xi_0 = \hat{\xi}_0\Omega_p^2$, and $\xi_2 = \hat{\xi}_2\Omega_p^2$ with Ω_p is made and

$$\alpha = \frac{3(R^3 - 2M^3)}{4M^3} \log\left(1 - \frac{2M}{R}\right) + \frac{3R^4 - 3R^3M - 2R^2M^2 - 8RM^3 + 6M^4}{2RM^2(R-2M)}. \tag{4.20}$$

It is to be noted that the expression for the Kepler frequency in Eq. (4.19) differs from that of Eq. (77) of Ref. [42]. This difference originates from the factor at the beginning of the third term within the second bracket and the term involving $\hat{\xi}_0$ and $\hat{\xi}_2$ in both equations. We discuss this issue further in the next section.

It is worth mentioning here that the model based on the slow rotation approximation is applicable for the fastest observed pulsar as noted by others [39, 42]. However, this approximation breaks down near the Kepler limit [39].

4.3 Results and Discussion

Now we discuss the results of slowly rotating superfluid neutron stars. Nonrotating background configurations are obtained by solving Eq. (4.6). In this context, we exploit the RMF EoS which includes the isospin dependent entrainment effect [40]. We use the GL and NL3 parameter sets in this calculation, both of which are listed in Table (3.1). Central neutron number density is an essential input for the calculation of the background configurations. The proton number density in the background model is no longer a free parameter

Table 4.1: The background nonrotating configurations for GL and NL3 sets as computed in chapter 3 are used here. Nucleon-meson coupling constants corresponding to the GL and sets are listed in Table 3.1. The central neutron wave number $k_n(0)$ is given by fm^{-1}. The mass(M) and radius (R) are in units of $M_\odot$ and km, respectively.

	$\nu(0)$	$k_n(0)$	$x_p(0)$	M	R	$\eta_0(0)$
GL	-2.38799	2.71	0.24	2.37	11.09	0.0
NL3	-2.33319	2.40	0.23	2.82	13.17	0.0

because the chemical equilibrium is imposed at the centre of the star, i.e., $\mu|_0 = \chi|_0$ [53]. The chemical equilibrium is established when both fluids are corotating. However, the chemical equilibrium does not hold good for different rotation rates of neutron and proton fluids [39, 66]. Masses and radii corresponding to two nonrotating configurations are also recorded in Table (4.1). The chosen background configurations are just below their maximum masses [40]. Furthermore, we consider $\eta_0(0) = 0$ and, consequently, $\Phi_0(0) = 0$ in all cases.

As soon as we know the background configuration, we can calculate the frame-dragging frequency from Eq. (4.9). As we are dealing with the two-fluid system, the central value of $\tilde{L}_n$ and relative rotation rate Ω_n/Ω_p are needed to solve Eq. (4.9) [42]. A rescaled Eq. (4.9) with the definition of $\hat{L}_n(r) = \tilde{L}_n/\Omega_p$ is solved to determine the frame-dragging frequency for different values of Ω_p using a fixed relative rotation rate. The boundary condition of the problem demands that the interior solution matches with the known vacuum solution given by Eq. (4.10). The frame-dragging frequency, $\frac{\omega(r)}{\Omega_p}$, is plotted as a function of radial

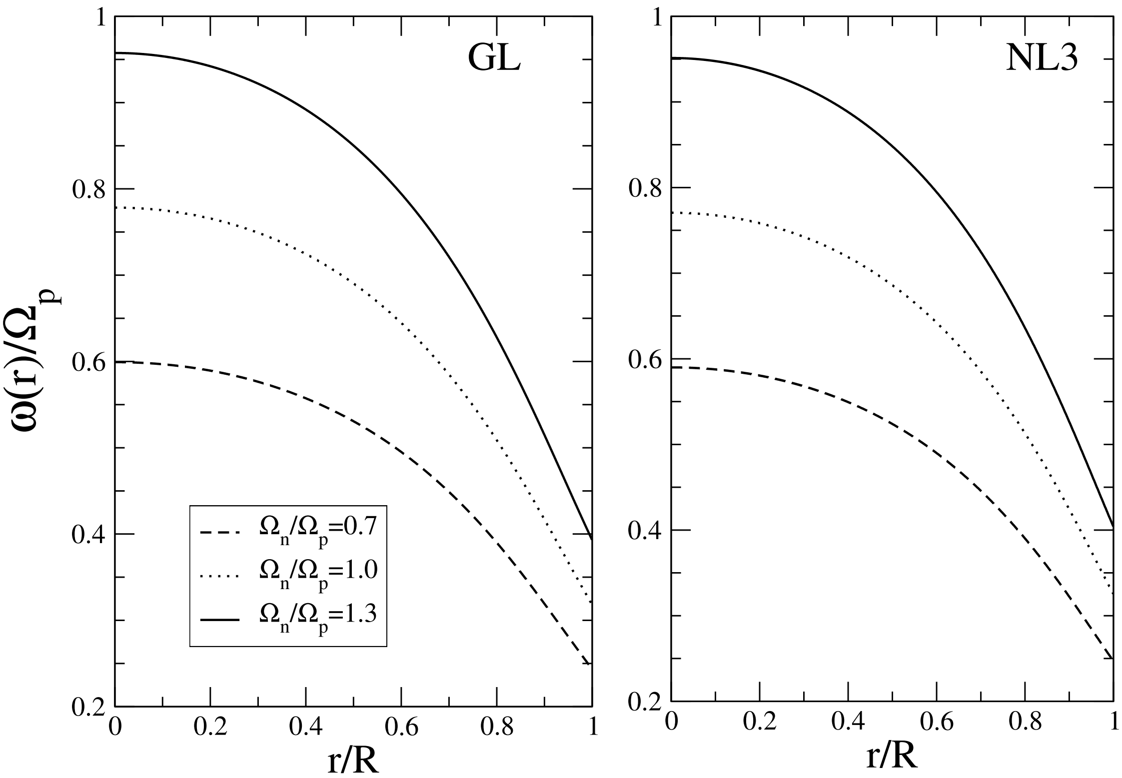

Figure 4.1: The frame-dragging frequency $\omega(r)$ is plotted as a function of radial distance (r/R) using the GL parameter set (left panel) and the NL3 parameter set (right panel) for three different relative rotation rates Ω_n/Ω_p [67].

distance (r/R) in Fig. (4.1) for three different relative rotation rates. The left panel denotes the GL parameter set and the right panel represents the NL3 set. The frame-dragging frequency decreases monotonically from the centre to the surface of the star for three relative rotation rates in both panels. This feature of the frame-dragging frequency is quite similar to the standard single-fluid result [69]. Further it is noted that the frame-dragging frequency is always higher for larger values of relative rotation rate.

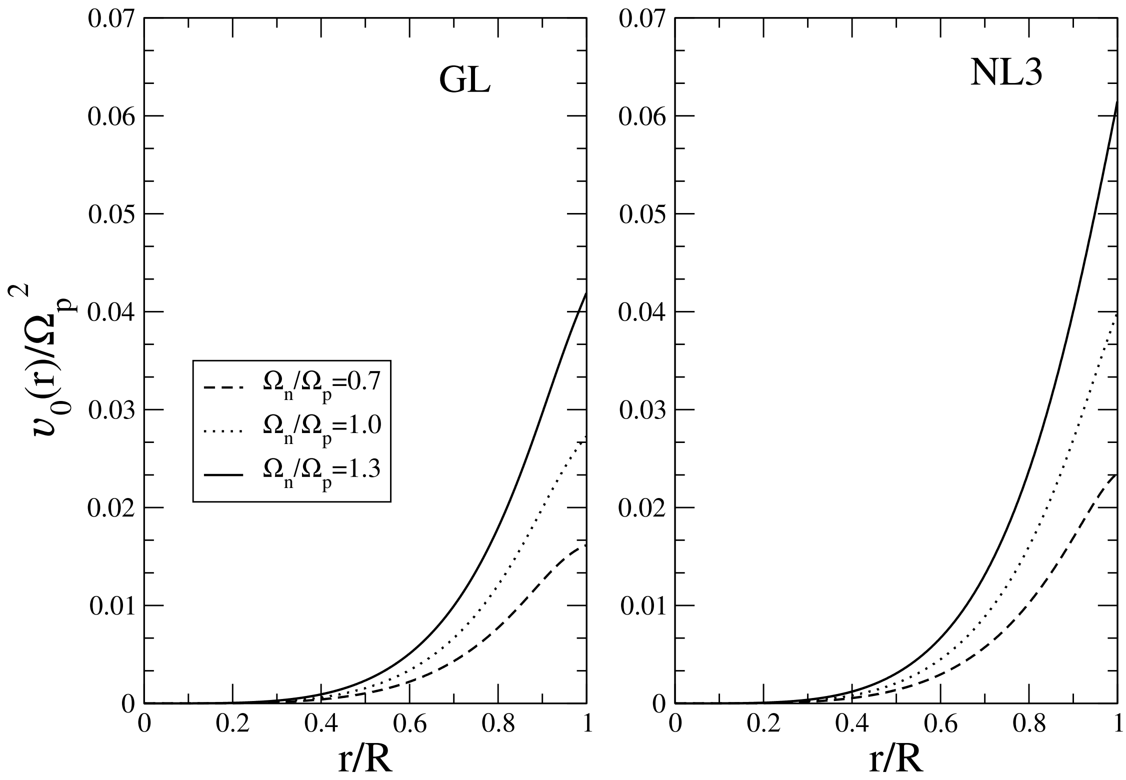

Figure 4.2: The metric function $v_0(r)$ is plotted as a function of radial distance (r/R) using the GL parameter set (left panel) and the NL3 parameter set (right panel) for three different relative rotation rates Ω_n/Ω_p [67].

Now we discuss numerical solutions of different metric functions of the superfluid neutron star in the slow rotation approximation . First we solve the $\ell = 0$ equations and determine ξ_0, η_0, Φ_0, h_0 and v_0 following the procedure laid down by Andersson and Comer [42]. Metric functions h_0 and v_0 match with the vacuum solutions at the surface. The metric function $v_0(r)$ as a function of radial distance is displayed in Fig. (4.2) for three different relative rotation rates. The left panel shows the results of the GL set and the right panel corresponds to those of the NL3 set. It is noted that the metric function v_0 increases

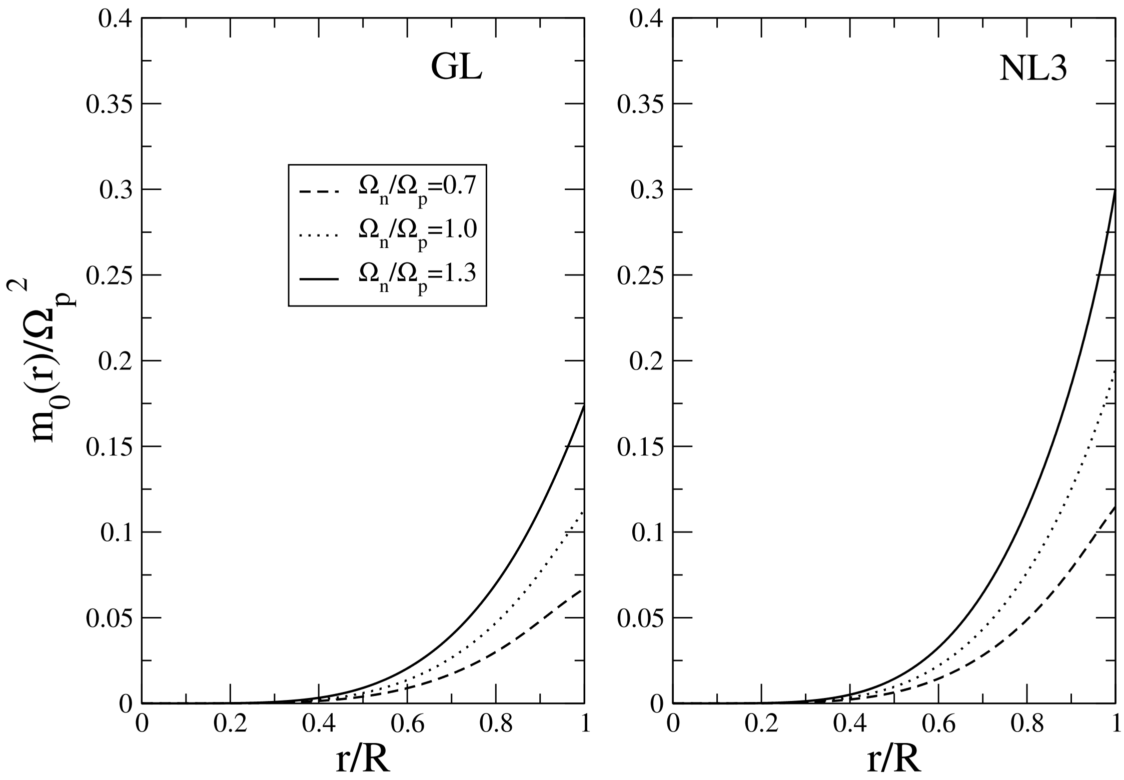

Figure 4.3: The metric function $m_0(r) = rv_0(r)/\exp(\lambda(r))$ is plotted as a function of radial distance (r/R) using the GL parameter set (left panel) and the NL3 parameter set (right panel) for three different relative rotation rates Ω_n/Ω_p [67].

monotonically to the surface and matches smoothly with the exterior solution. For the NL3 set, the value of this metric function at the surface is always higher than that of the GL set. A new metric function m_0 is defined in terms of v_0 and λ as $m_0 = rv_0/\exp(\lambda)$. The radial profile of m_0, which merges with the exterior solution at the surface, is shown in Fig. (4.3) for different relative rotation rates.

We solve the $\ell = 2$ equations in a similar way to that used for solutions of $\ell = 0$ equations [42]. A new variable, $\bar{k} = k_2 + h_2$, is introduced to solve two coupled first-

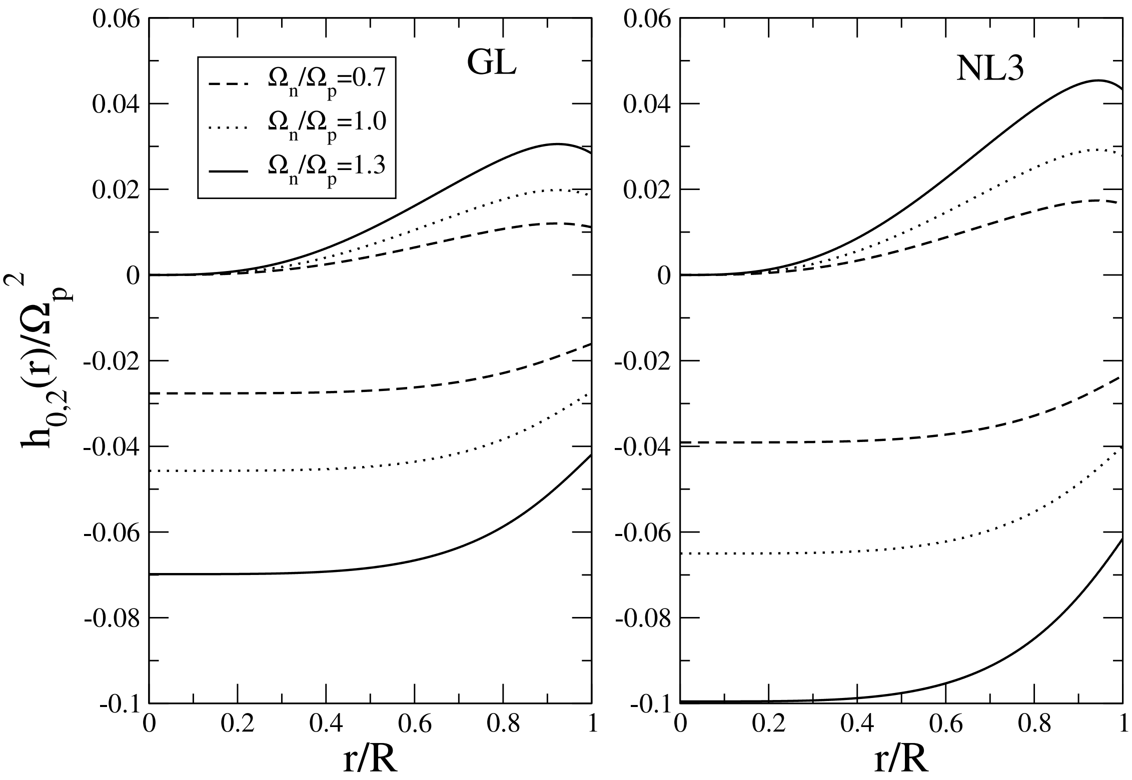

Figure 4.4: The metric functions $h_0(r)$ (three lower curves) and $h_2(r)$ (three upper curves) are plotted as a function of radial distance (r/R) for three different relative rotation rates Ω_n/Ω_p. The left panel shows the results of the GL parameter set and the right panel demonstrates those of the NL3 parameter set [67].

order equations in h_2 and k_2 [68]. This leads to two coupled differential equations in $\bar{k}$ and h_2, which are solved using the method described by Hartle [68]. In Fig. (4.4) , the metric functions h_0 and h_2 are plotted as a function of radial distance for different relative rotation rates. The results of the GL and NL3 sets are shown in the left and right panels, respectively. In both panels, the lower three curves denote the metric function h_0 and the upper three curves imply the metric function h_2. Figure (4.5) shows the radial profiles of

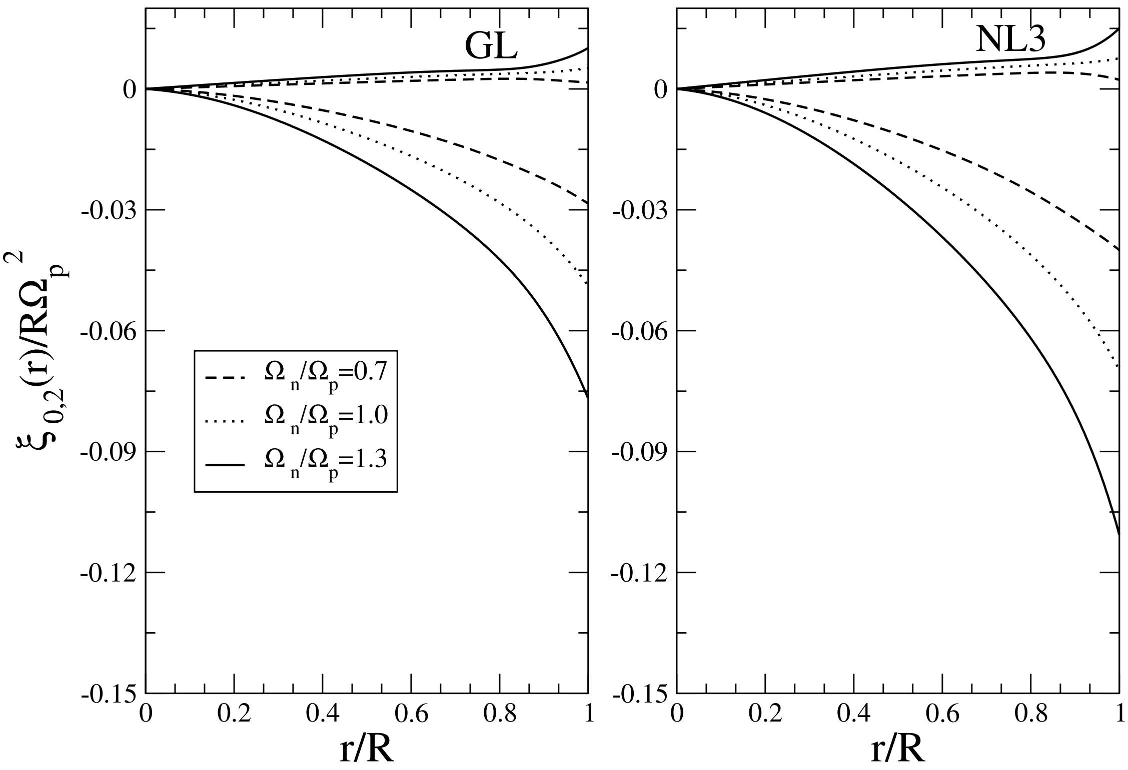

Figure 4.5: The radial displacement $\xi_0(r)$ (three upper curves) and $\xi_2(r)$ (three lower curves) are plotted as a function of radial distance (r/R) for three different relative rotation rates Ω_n/Ω_p. The left panel shows the results of the GL parameter set and the right panel represents those of the NL3 parameter set [67].

$\xi_0(r)$ (upper curves) and $\xi_2(r)$ (lower curves), and in Fig. (4.6), we have $\bar{k} = k_2 + h_2$ versus r for the GL (left panel) and NL3 (right panel) sets and three different relative rotation rates. In Fig. (4.5) , the magnitude of $\xi_2(r)$ at the surface in the right panel is quite large with respect to that of the left panel when the relative rotation rate is larger than 1 and this function is directly related to the deformation of the star due to rotation.

Figure (4.7) exhibits the variation of rotationally induced corrections to the neutron number density $n_0\eta_0$ (three upper curves) and $n_0\eta_2$ (three lower curves) with radius. Sim-

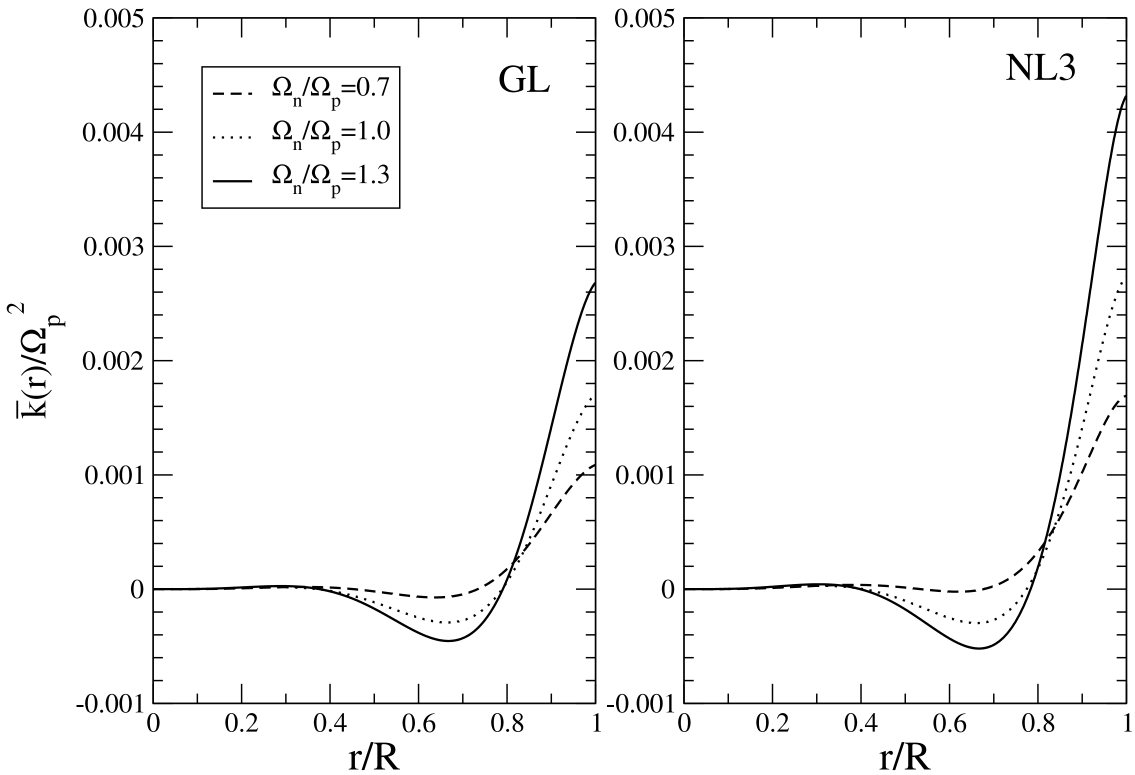

Figure 4.6: The quantity $\bar{k}$ is plotted as a function of radial distance (r/R) using the GL parameter set (left panel) and NL3 parameter set (right panel) for three different rotation rates Ω_n/Ω_p [67].

ilarly, Fig. (4.8) represents the variation of rotationally induced corrections to the proton number density $p_0\Phi_0$ (three upper curves) and $p_0\Phi_2$ (three lower curves) with radius. In both cases, the left panel denotes the results of the GL set and the right panel corresponds to those of the NL3 set. We explore the role of symmetry energy on the rotationally induced corrections to the proton number density by comparing two cases with (left panel) and without (right panel) ρ mesons for the GL set in Fig. (4.9). For the case without ρ mesons, we consider a nonrotating configuration that is just below the maximum mass neutron star. The mass and radius of this neutron star are 2.33 $M_\odot$ and 10.96 km, respectively. It is noted

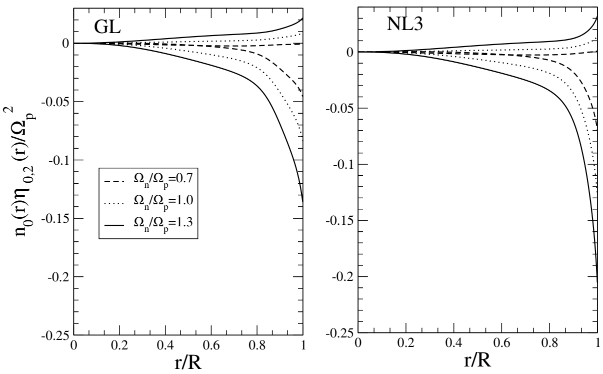

Figure 4.7: The rotationally induced corrections to the neutron number density $n_0(r)\eta_0(r)$ (three upper curves) and $n_0(r)\eta_2(r)$ (three lower curves) are plotted as a function of radial distance (r/R) for three different relative rotation rates Ω_n/Ω_p. Results of the GL and NL3 parameter sets are shown in the left and right panels, respectively [67].

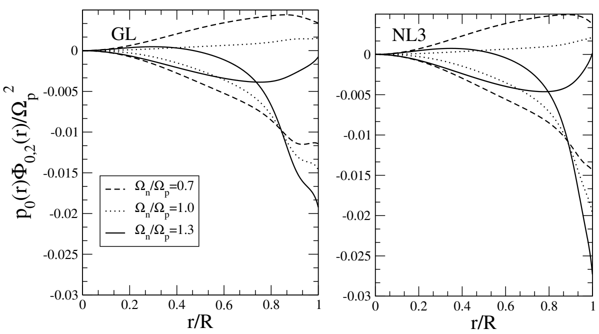

Figure 4.8: The rotationally induced corrections to the proton number density $p_0(r)\phi_0(r)$ (three upper curves at $r/R = 1$) and $p_0(r)\phi_2(r)$ (three lower curves at $r/R = 1$) are plotted as a function of radial distance (r/R) using the GL parameter set (left panel) and NL3 parameter set (right panel) for three different relative rotation rates Ω_n/Ω_p [67].

that the corrections to the proton number density are significantly modified in the presence of ρ mesons.

The deformation of a rotating star is obtained in terms of the ratio of the polar and equatorial radii. For the slowly rotating star, this is given by $\frac{R_p}{R_e} \approx 1 + \frac{3\xi_2(R)}{2R}$. The ratio

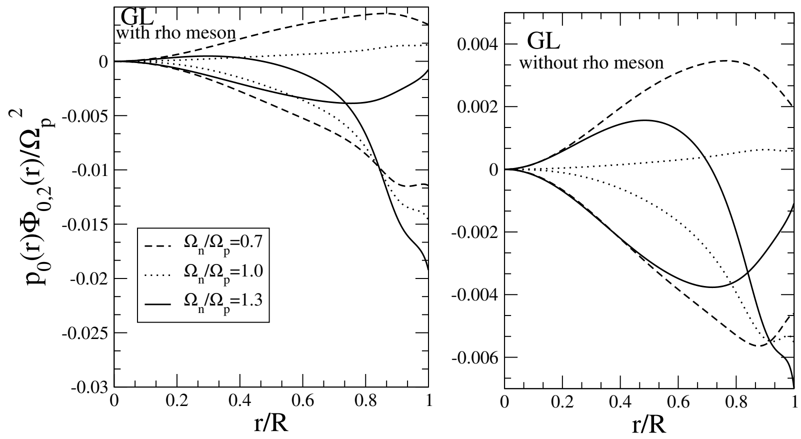

Figure 4.9: The rotationally induced corrections to the proton number density $p_0(r)\phi_0(r)$ (three upper curves at $r/R = 1$) and $p_0(r)\phi_2(r)$ (three lower curves at $r/R = 1$) are plotted as a function of radial distance (r/R) for the GL parameter set with (left panel) and without (right panel) ρ mesons for three different relative rotation rates Ω_n/Ω_p [67].

of polar to equatorial radii as a function of relative rotation rate is plotted in Fig. (4.10) for the GL (solid line) and NL3 (dashed line) sets. We consider the proton rotation rate to be equal to that of the fastest rotating pulsar having spin frequency 716 Hz [70]. The nonrotating situation is achieved when the relative rotation rate approaches zero. Furthermore we find that the rotationally induced deformation of the star is larger for the NL3 case than the GL case. This deformation increases with increasing relative rotation rate. As neutron and proton fluids may rotate at different rates, one of them extends beyond the other at the equator. The Kepler limit is obtained from the rotation rate of the outer fluid. To determine the mass-shedding (Kepler) limit we have to solve the quadratic equation (4.19) for Ω_p. When $\Omega_n > \Omega_p$ the Kepler frequency is determined by the neutrons; for $\Omega_p > \Omega_n$, the Kepler frequency is determined by the protons. We calculate the Kepler limit in the RMF model including ρ mesons using the GL and NL3 parameter sets for the background configurations of Table (4.1). The mass-shedding (Kepler) limit Ω_K as a function

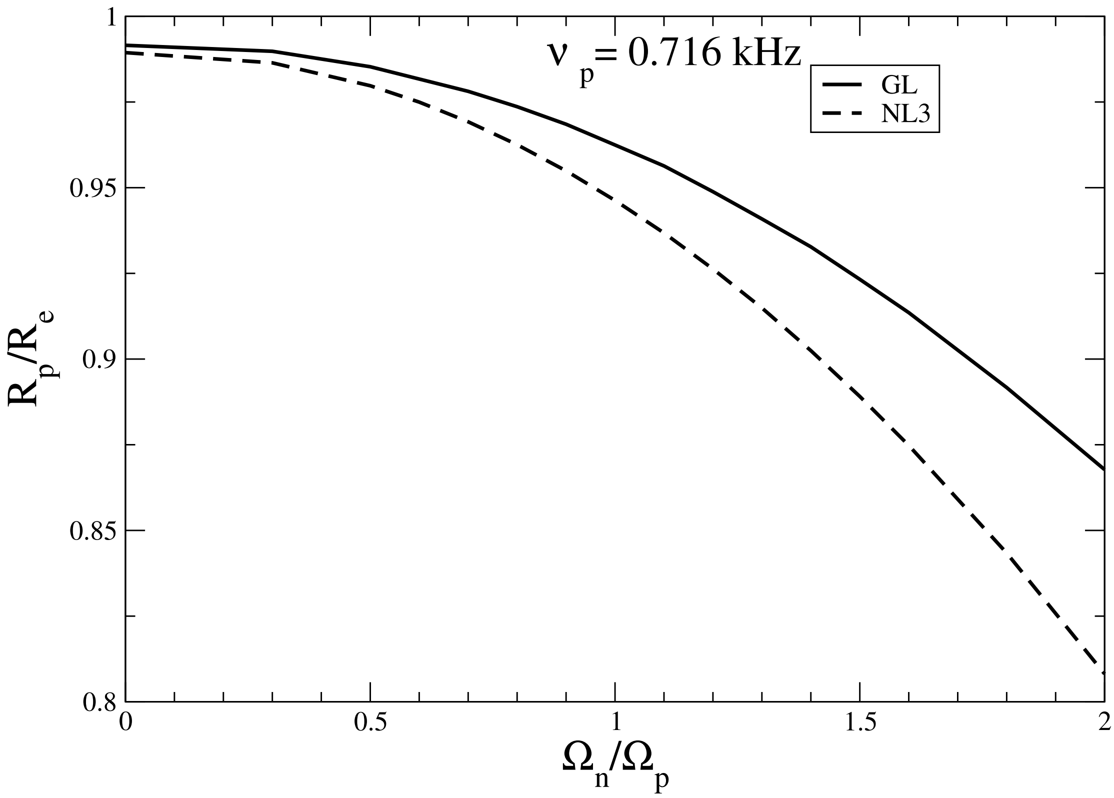

Figure 4.10: The ratio of the polar to equatorial radii (R_p/R_e) is shown as a function of relative rotation rate Ω_n/Ω_p corresponding to neutron stars of masses 2.37 $M_\odot$ with the GL set (solid line) and 2.82 $M_\odot$ with the NL3 set (dashed line), respectively, considering that $\nu_p = \Omega_p/2\pi$ is equal to that of the fastest rotating pulsar having spin frequency 716 Hz [70] [67].

of relative rotation rate is plotted in Fig. (4.11) for the GL set (left panel) and the NL3 set (right panel). We use the radial profiles of the entrainment effect in this calculation of Kepler frequency. The results are qualitatively similar to the previous investigation by Prix and collaborators [39] though the authors in the that case used some constant values of entrainment. However, our results are different from those of Comer [61]. For $\Omega_n > \Omega_p$, the Kepler frequency (solid square) approaches a constant value with increasing Ω_n. When $\Omega_n/\Omega_p < 1$, the Kepler frequency (solid circle) monotonically increases with decreasing

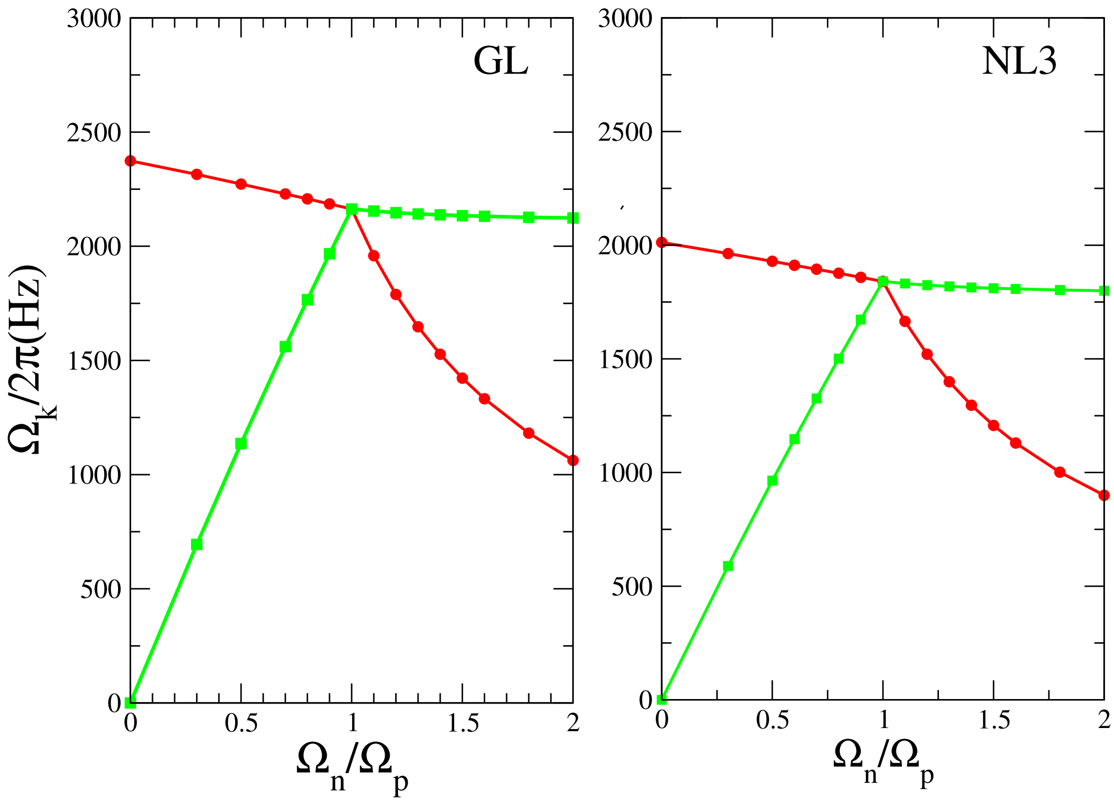

Figure 4.11: The mass-shedding (Kepler) limit is shown as a function of relative rotation rate Ω_n/Ω_p for the GL set (left panel) and the NL3 set (right panel). The solid squares (green) show the allowed rotation rate of the neutron fluid (Ω_n) and the solid circles (red) show the allowed rotation rate of the proton fluid (Ω_p). The Kepler frequency is the largest of the two [67].

relative rotation rate, as evident from Fig. (4.11), whereas the opposite scenario was found in the work of Comer [61]. On the other hand, Prix *et al.* [39] found that the Kepler limit increased monotonically as the relative rotation rate decreased. This is quite similar to our results. The difference between our results and those of Comer [61] may be due to different expressions for Ω_K that we have discussed in connection with Eq.(4.19) in Sec. (4.2). Furthermore, Comer [61] calculated the entrainment using the equation of state obtained in the relativistic σ-ω model. Without ρ mesons, the effects of symmetry energy on the entrainment was absent. On the other hand, we exploit an isospin dependent entrainment effect calculated in the σ-ω-ρ RMF model for the determination of the Kepler limit [40]. We compare the Kepler limit calculated in the RMF model with and without ρ mesons for the GL set in Fig. (4.12). In both cases, we consider nonrotating configurations that are just below their maximum masses, as noted in Table (4.1) and discussed in connection with Fig. (4.7). The solid line denotes the calculation without ρ mesons and the dashed line represents the case with ρ mesons. Furthermore, solid squares and circles correspond to allowed rotation rates of neutron and proton fluids, respectively. It is noted that the two results differ, as is evident from the highlighted part of Fig. (4.12).

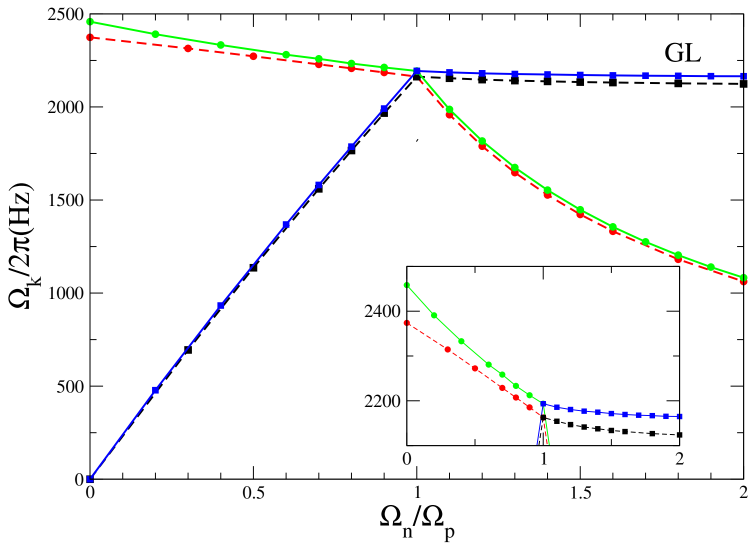

Figure 4.12: (Color online) The mass-shedding (Kepler) limit is shown as a function of relative rotation rate Ω_n/Ω_p with (dashed line) and without ρ mesons (solid line) for the GL set. The solid squares show the allowed rotation rate of the neutron fluid (Ω_n) and the solid circles show the allowed rotation rate of the proton fluid (Ω_p) [67].

4.4 Summary and Conclusions

In chapter 4, we have studied the role of the isospin dependent entrainment and the relative rotation rates of neutron and proton fluids on the global properties of slowly rotating superfluid neutron stars such as the structures and the Kepler limit in the two-fluid formalism. The two-fluid formalism of Andersson and Comer [61] is adopted in our work. The effects of symmetry energy on the EoS and entrainment are studied using the σ-ω-ρ RMF model. The symmetry energy significantly influences the rotationally induced corrections to the proton number density. It is found that the Kepler limit obtained with the isospin dependent entrainment effect is lower than that of the case when the isospin term is neglected in the entrainment effect. The behaviour of the Kepler limit as a function of the relative rotation rate in our case is qualitatively similar to the results of Prix *et al.* [39] obtained using the polytropic EoS. The calculation of slowly rotating superfluid neutron stars including the isospin dependent entrainment effect in a realistic EoS is the first of its kind.

Our calculation may be extended to investigate the superfluidity in neutron star matter including Λ hyperons and its consequence on the superfluid moment of inertia in explaining pulsars glitches as well as the rapid cooling of the neutron star in Cas A. For this Λ hyperons could be treated as a superfluid and become part of the neutron fluid in the two-fluid formalism. The change in the observed spin due to glitches may be calculated using the two fluid model. This might reveal the role of the core superfluid moment of inertia on pulsar glitches.

BIBLIOGRAPHY

[1] J. Antoniadis et al., Science **340**, 1233232 (2013).

[2] F. Ozel, Nature **441**, 1115 (2006).

[3] Haensel, P., Potekhin, A.Y., and Yakovlev, D.G., Neutron Stars 1: Equation of State and Structure, Astrophysics and Space Science Library, vol. 326, (Springer, New York, U.S.A., 2007).

[4] N. K. Glendenning, Compact Stars, (Springer-Verlag, New York, 1997).

[5] D. G. Ravenhall, C. J. Pethick and J. R. Wilson, Phys. Rev. Lett. **50**, 2066 (1983).

[6] K. Oyamatsu, Nucl. Phys. A **561**, 431 (1993).

[7] J. M. Lattimer , M. Prakash.,Science **23**, 304, 5670(2004) .

[8] S. E. Thorsett and Deepto Chakrabarty, ApJ **512**, 288(1999)

[9] I. I. Shapiro, Phys. Rev. Lett. **26**, 789 (1964).

[10] J.M. Weisberg, J.H. Taylor, in Radio Pulsars, M. Bailes, D.J. Nice, S.E. Thorsett, Eds. (Astron. Soc. Pac. Conf. Ser. 302, San Francisco, 2003).

[11] A.G. Lyne et al., Science **303**, 1153 (2004).

[12] A. B. Migdal, Soviet Physics JETP **10**, 176 (1960).

[13] G. Baym, C. J. Pethick, and D. Pines, Nature **224**, 673 (1969).

[14] C. H. Yang and J. W. Clark, Nucl. Phys A **174**, 49 (1971).

[15] C.-H. Yang and J. W. Clark, Nuovo Cimento Lett. **3**, 272 (1970).

[16] N. C. Chao, J. W. Clark, and C.-H. Yang, Nucl. Phys. A **179**, 320 (1972).

[17] M. Hoffberg, A. E. Glassgold, R. W. Richardson, and M. Ruderman, Phys. Rev. Lett. **24**, 775 (1970).

[18] T. Takatsuka, Prog. Theor. Phys. **48**, 1517 (1972).

[19] Yakovlev, D.G., K.P. Levenfish and Yu.A. Shibanov, 1999, Cooling of neutron stars and superfluidity in their cores.

[20] Armen Sedrakian, John W Clark and Mark Alford, 2006, ”Pairing in Fermionic Systems: Basic Concepts and Modern Applications”, World Scientific.

[21] D. G. Yakovlev, C. J. Pethick, Ann. Rev. A&A **42**, 169 (2004).

[22] D. J. Dean et al. , Rev. of Mod. Phys, **75** 607 (2003).

[23] Baldo, M., Ø. Elgary, L. Engvik, M. Hjorth-Jensen, and H.J. Schulze, Phys. Rev. C **58**, 1921(1998).

[24] C.O. Heinke and W.C.G. Ho, Astrophys. J. Lett. **719**, L167 (2010).

[25] D. Page, M. Prakash, J.M. Lattimer and A.W. Steiner, Phys. Rev. Lett. **106**, 081101 (2011).

[26] S. Shternin *et al.*, Mon. Not. R. Astron. Soc. **412**, L108 (2011).

[27] Blaschke *et al.*, Phys. Rev. C **85**, 022802 (2012).

[28] A. Sedrakian, Astron. Astrophys. **555**, L10 (2013).

[29] A. G. Lyne, S. L. Shemar, and F. G. Smith, Mon. Not. Roy. Astr. Soc.**315**, 534 (2000).

[30] N. Andersson, K. Glampedakis, W.C.G. Ho, and C.M. Espinoza, Phys. Rev. Lett. **109**, 241103 (2012).

[31] N. Chamel, Phys. Rev. Lett. **110**, 011101 (2013).

[32] G. Baym, C.J. Pethick, D. Pines and M. Ruderman, Nature (London) **224**, 872 (1969).

[33] P.W. Anderson and N. Itoh, Nature (London) **256**, 25 (1975).

[34] A.F. Andreev and E.P. Bashkin, Zh. Eksp. Teor. Fiz. **69**, 319 (1975)[Sov. Phys. JETP **42**, 164 (1976)].

[35] D. M. Sedrakyan, K. M. Shakhabasyan, and A. G. Movsisyan, Astrofizka, Vol. 19, No. 2, PP. 303-314, (1983).

[36] N. Andersson, G.L. Comer and D. Langlois, Phys. Rev. D **66**, 104002 (2002).

[37] N. Andersson and G.L. Comer, Mon. Not. R. Astron. Soc. **328**, 1129 (2001).

[38] N. Andersson, G.L. Comer and R. Prix, Phys. Rev. Lett. **90**, 091101 (2003).

[39] R. Prix, G.L. Comer, and N. Andersson, Astron. Astrophys. **381**, 178 (2002).

[40] A. Kheto and D. Bandyopadhyay, Phys. Rev. D **89**, 023007 (2014).

[41] B. Carter, in Relativistic Fluid Dynamics, edited by A. Anile and M. Choquet-Bruhat (Springer, Heidelberg, 1989).

[42] N. Andersson and G.L. Comer, Classical Quantum Gravity **18**, 969 (2001).

[43] G.L. Comer, Found. Phys. **32**, 1903 (2002).

[44] G.L. Comer and D. Langlois, Classical Quantum Gravity **11**, 709 (1994).

[45] B. Carter and D. Langlois, Phys. Rev. D **51**, 5855 (1995).

[46] B. Carter and D. Langlois, Nucl. Phys. **B531**, 478 (1998).

[47] D. Langlois, A. Sedrakian and B. Carter, Mon. Not. R. Astron. Soc. **297**, 1189 (1998).

[48] N. Andersson and G.L. Comer, Living Rev. Relativity **10**, 1 (2007).

[49] J D Walecka, Ann. of Phys. **83**, 491 (1974).

[50] J. Boguta and A.R. Bodmer, Nucl. Phys. **A292**, 413 (1977).

[51] C. W. Misner, K. S. Thorne, and J. A. Wheeler, *Gravitation* (Freeman Press, San Francisco, 1973).

[52] G. Comer and R. Joynt, Phys. Rev. D **68**, 023002 (2003).

[53] G. Comer, D. Langlois and L. M. Lin, Phys. Rev. D **60**, 104025 (1999).

[54] L. Lindblom and G. Mendell, Phys. Rev. D **61**, 104003 (2000).

[55] M. Borumand, R. Joynt and W. Klúzniak, Phys. Rev. C **54**, 2745 (1996).

[56] O. Sjoberg, Nucl. Phys. A **265**, 511 (1976).

[57] N. Chamel and P. Haensel, Phys. Rev. C **73**, 045802 (2006).

[58] N. Chamel, Mon. Not. R. Astron. Soc. **388**, 737 (2008).

[59] M.E. Gusakov and P. Haensel, Nucl. Phys. **A761**, 333 (2005).

[60] M.E. Gusakov, E.M. Kantor and P. Haensel, Phys. Rev. C **79**, 055896 (2009).

[61] G. Comer, Phys. Rev. D **69**, 123009 (2004).

[62] F.J. Fattoyev, C.J. Horowitz, J. Piekarewicz and G. Shen, Phys. Rev. C **82**, 055803 (2010).

[63] R. Prix and M. Rieutord, Astron. Astrophys. **393**, 949 (2002).

[64] G.A. Lalazissis, J. König and P. Ring, Phys. Rev. C **55**, 540 (1997).

[65] M.E. Gusakov, E.M. Kantor and P. Haensel, Phys. Rev. C **80**, 015803 (2009).

[66] R. Prix, J. Novak and G.L. Comer, Phys. Rev. D **71**, 043005 (2005).

[67] A. Kheto and D. Bandyopadhyay, Phys. Rev. D **91**, 043006 (2015).

[68] J. B. Hartle, Astrophys. J. **150** ,1005 (1967).

[69] J. B. Hartle and K. S. Thorne, Astrophys. J.**163**, 807 (1968).

[70] J. W. Hessels et al., Science **311**, 1901 (2006).